The Rift and Continent-Ocean Transition Structure Under the Tagus Abyssal Plain West of the Iberia

I. Merino[1], C. R. Ranero[1,2], M. Prada[1], V. Sallarès[1], and I. Grevemeyer[3]

[1]Barcelona Center for Subsurface Imaging, ICM, CSIC, Barcelona, Spain, [2]Barcelona Center for Subsurface Imaging, ICM, ICREA at CSIC, Barcelona, Spain, [3]GEOMAR Helmholtz Centre for Ocean Research Kiel, Kiel, Germany

Abstract The West Iberia margin is the focus of intense research since the 1980s, with some of the most exemplary geophysical cross-sections and drilling expeditions. Those data sets have been used to create conceptual models of rifting used as a template to interpret margins worldwide. We present two collocated ∼350 km long lines of multi-channel seismic (MCS) streamer data and wide-angle seismic (WAS) data collected across the Tagus Abyssal Plain (TAP). We use travel-times of first arrivals identified at WAS and reflected seismic phases identified at both WAS and MCS records to jointly invert for the *P* wave velocity (*V*p) distribution and the geometry of a sediment unconformity, the top of the basement, and the Moho boundary. The *V*p model shows that the TAP basement is more complex than previously inferred, presenting abrupt boundaries between five domains. Domain I under the foot of the slope and Domain III under the abyssal plain display *V*p values and gradients of thin continental crust. In between, Domain II displays a steep *V*p gradient and high *V*p values at shallow depth that support that basement is made of exhumed partly serpentinized mantle. Domain IV and Domain V, further oceanward, have oceanic crust *V*p structure. The new results support an unanticipated complex rift history during the initial separation of Iberia and America. We propose a geodynamic scenario characterized by two phases of extension separated by a jump of the locus of extension, caused by the northward propagation of the oceanic spreading center during the J-anomaly formation, which terminated continental rifting.

Plain Language Summary The underground offshore of Western Iberia has been studied since the early 1980s to understand the mechanism that formed the North Atlantic Ocean around 200 million years ago. Some of the geophysical experiments carried on in this area have been used to created conceptual models that explain the opening of this region. Here, we present two new geophysical data sets to explore the Tagus Abyssal Plain (TAP), located in front of south Portugal, and to understand how the ocean opened up in this region. The integration of these two data sets allows us to create a seismic velocity model which decreases the uncertainty on the final interpretation regarding the origin of the TAP. The model from our study reveals that the TAP structure is more complex than previously proposed. We explain the new configuration by making the hypothesis that the ocean opens in two distinct and independent phases of extension. This is in contrast to the classical theories that states that the opening of this ocean took place progressively, in a unique episode of extension.

1. Introduction

Rifted continental margins are regions where extension processes led to continental extension, breakup, and seafloor spreading with the formation of oceanic crust. However, off Iberia continental breakup is not characterized by a sharp boundary but by a ∼100 km broad (e.g., Dean et al., 2000; Pickup et al., 1996) often rather complex transition zone, called the continent-ocean transition or COT. Ground truthing with deep drilling revealed that the COT is made of mantle exhumed by extensional processes along the entire West Iberia margin (Boillot et al., 1987; Ryan et al., 1973; Sawyer et al., 1994). In addition, geophysical efforts determined heterogeneity of the structure, rock physical properties, and tectonic style of the basement at a regional scale, defining the location and nature of the COT and the oldest oceanic crust (Whitmarsh et al., 1998). As a result, the West Iberia continental margin and COT became the type example of magma-poor systems that has been used as a template to interpret the structure of many other rifted systems where less information of the nature of the basement is available.

However, most experiments studied the Galicia Segment of the northern West Iberia margin (Dean et al., 2015; Pérez-Gussinyé et al., 2003; Whitmarsh et al., 1996) or the Iberia Abyssal Plain (IAP) in the central region of the margin (Dean et al., 2000; Grevemeyer et al., 2019; Minshull et al., 2014). The most accepted models of the COT in this area involve mantle unroofing, typically postulating a continuum from continental crust extension, continental mantle exhumation over wide areas and the subsequent forma-tion of oceanic crust (e.g., Pérez-Gussinyé et al., 2006). Driving mechanisms of those processes are mantle serpentinization weakening the lithosphere and promoting continental crust break up (Pérez-Gussinyé & Reston, 2001) and by increasing rates of extension causing mantle decompression melting that led to a new spreading center (Whitmarsh et al., 2001).

Zones of mantle exhumation have also been postulated within the COT on its conjugate margins, landward of unequivocal oceanic crust (e.g., Dean et al., 2000; Van Avendonk et al., 2006). In spite of the number of geophysical experiments, the typical seismic structure of normal oceanic crust has not yet been clearly detected along the margin and its conjugate sibling off Newfoundland.

Yet, a major part of the Iberia margin has not been studied in detail, namely the Tagus Abyssal Plain (TAP) to the south of IAP and previous studies provided only a low-resolution characterization (see Figure 1, IAM5 with only 3 OBS spaced ∼30–40 km, Afilhado et al., 2008) on the extent and structure of the conti-nental crust and COT in the TAP.

This work aims at defining the petrological affinity, i.e., the nature, of the transitions between the different basement domains across the TAP, showing for the first time the structure of the oceanic crust formed in the north Atlantic and the mechanism that produces the final breakup. Here, we use high-resolution struc-tural models obtained from jointly interpreting wide-angle seismic (WAS) and gravity data combined with multi-channel seismic (MCS) images. Specifically, we present results from a ∼450 km long WAS and gravity profile and a coincident MCS line acquired across the TAP, at ∼38°N (Figure 1b). We obtained a 2-D Vp tomography model along the FRAME-2 line by jointly inverting refraction and reflection TT from the WAS and MCS data (Figure 3a), which is then validated with gravity modeling. The MCS image is subsequently used to help defining the crustal structure and boundaries between interpreted petrological domains.

2. Geological Setting

The Iberia-Newfoundland rift system initiated the opening of the North Atlantic Ocean. The age of con-tinental breakup and the onset of seafloor spreading between the two conjugated margins is inferred to decrease northward along the margin but the details are debated (e.g., Bronner et al., 2011; Reston & Mor-gan, 2004). The J-anomaly (M0-M4) has a well-defined oceanic origin in the African-American plates of the Central Atlantic (e.g., Rovere et al., 2004). However, the literature from the West Iberia still debates its origin and proper individual M-series lineations have never been identified in this region. Some scientists suggest an oceanic origin (Russell & Whitmarsh, 2003; Srivastava et al., 2000) but other propose that it is related to synrift magmatism (Bronner et al., 2011; Nirrengarten et al., 2017).

In the SW segment, a WAS profile (P1 in Figure 1) provides strong evidence for the presence of serpen-tinized mantle of Early Cretaceous age extending from the Gorringe Bank (Ryan et al., 1973) under the southern TAP and northern Horseshoe Abyssal Plain (HAP; Sallarès et al., 2013). In the central Gulf of Cadiz and Seine Abyssal Plain lines P1 and P2 found oceanic crust (Figure 1; Martínez-Loriente et al., 2014; Sallarès et al., 2011).

However, the information on the configuration, nature, and limits between the crustal domains in the TAP is scarce and mostly based on the modeling of a collection of vintage geophysical data (Pinheiro et al., 1992; Purdy, 1975; see Figure 1) and of a WAS profile from the nineties with three ocean bottom seismometers (OBS) coincident with MCS line IAM-5 (Afilhado et al., 2008, see Figure 1).

The results of seismic refraction line A–AR (Purdy, 1975, see Figure 1) in the south segment of the Ibe-ria margin indicated major changes in velocity and thickness of crustal layers within the deep basin. In particular, those data were interpreted as corresponding to oceanic crust in the external part of the Gulf of Cadiz. Farther SW of the TAP, across the Madeira-Tore Rise, the presence of the J-anomaly magnetic lineation (Tucholke & Ludwig, 1982) supports the presence of oceanic crust. The Vp model from Peirce and
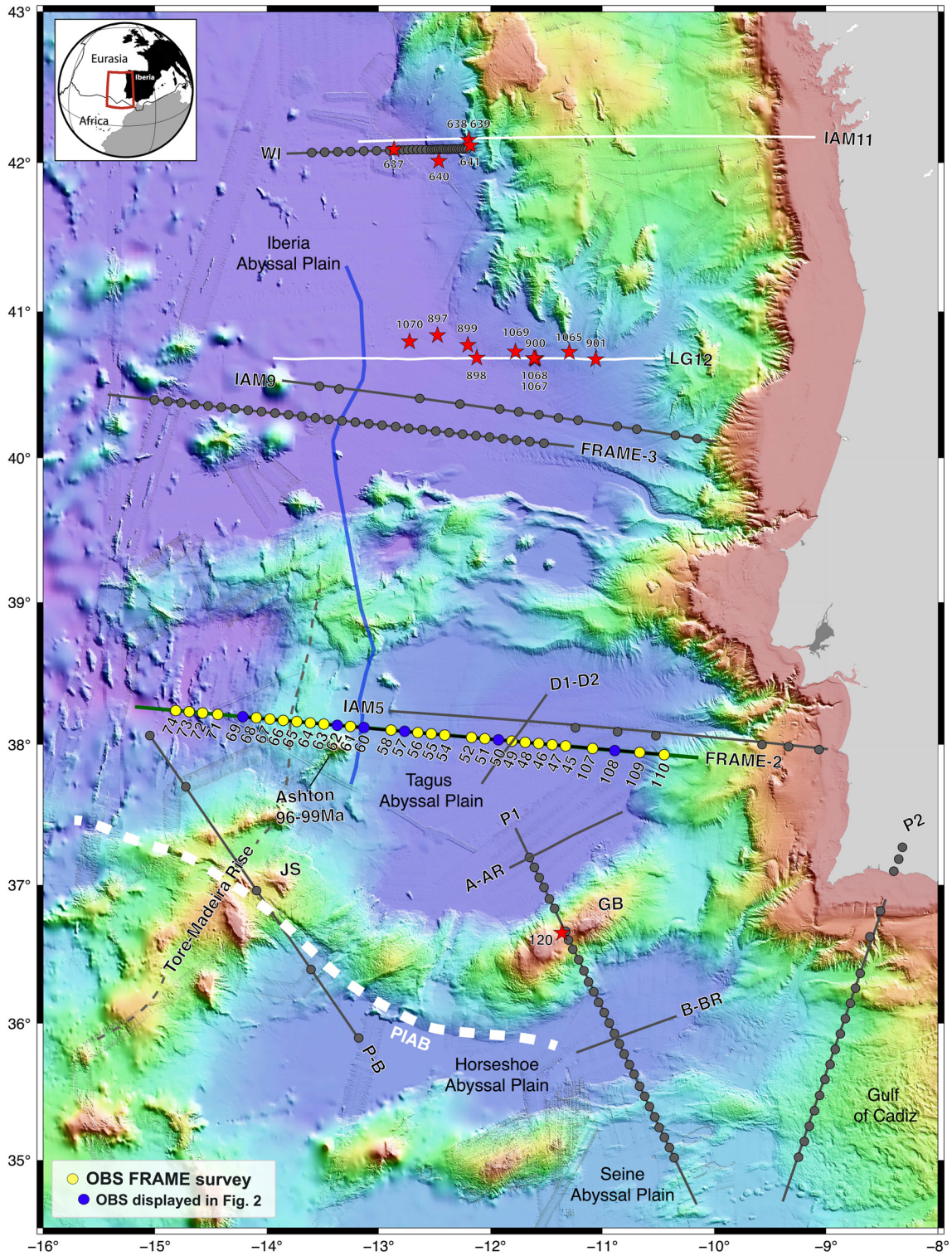
Figure 1.

Barton (1991) of the Josephine Seamount and the Madeira-Tore Rise, shows a crust having a total thickness of ~14–16 km and Vp values of 7.4 km/s in the lowest part. They suggest that it consists of anomalous oceanic crust. To explain the anomaly in thickness and velocity, they propose the addition of igneous material at the base of the crust with an anomalously low MgO abundance. Furthermore, they suggest that this oceanic crust formed as part of an aseismic ridge at or adjacent to the Mid-Atlantic Ridge.

Pinheiro et al. (1992) modeled WAS data of profile D1-D2 (Figure 1) and document evidence of a high-velocity basement with Vp of 7.6–7.9 km/s showing a strong vertical velocity gradient that is consistent with the possible presence of exhumed and serpentinized mantle under the TAP, from 11.5° to 12°W, which they interpreted to correspond to the COT. Based on a grid of seismic images, Mauffret et al. (1989) proposes a Mesozoic-Cenozoic seismic stratigraphy. They interpreted that the whole TAP is underlain by oceanic crust, and proposed an ocean-continent boundary at ~11°W, near the foot of the continental slope. They interpret that the deep basement beneath the eastern TAP was created in Late Jurassic time followed by a Cretaceous ridge jump that left oceanic crust adjacent to the continental Iberian margin.

For long time, the most modern geophysical transect across the TAP was the Iberian Atlantic Margins line 5 (IAM-5) that was shot and recorded on streamer by an industry ship and had 6 OBS deployed during acquisitions. Only 3 of the OBS were located on the floor of the abyssal plain, with a lateral spacing of 30–40 km, and the other 3 across the uppermost slope and shelf (Figure 1). The arrivals in the OBS records and selected horizons from the seismic boundaries were forward modeled and interpreted together with magnetic data (Afilhado et al., 2008). They interpret a ~40 km wide segment of highly reflective and slightly magnetized "transitional crust" extending under the continental slope and eastern sector of the TAP, and proposed that it corresponds to the COT. They inferred the presence of oceanic crust further to the west under the TAP. Further west, they identified magnetic anomalies from the M-series suggesting seafloor spreading. WAS data acquired in 1963 along the Tagus and HAPs using sonobuoys (lines A-AR and B-BR in Figure 1; Purdy, 1975) had previously been interpreted as showing oceanic crust in the Horseshoe and TAP.

3. Data Sets

The MCS and WAS data used in this work were acquired during the FRAME (*FoRmAtion of geological domains in the Western Iberian Margin and tectonic rEactivation of their limits*) experiment in 2018, conducted on board the Spanish R/V Sarmiento de Gamboa. The FRAME experiment aimed at providing new insights into the spatial distribution of geological domains to characterize the COT offshore Iberia, and improve our understanding of the processes that have shaped the margin. Here, we use data acquired along the FRAME-2 transect, which runs E-W from 10° to 15° of longitude across the TAP and the J-anomaly ridge (Figure 1). The experiment combines a ~330 km long MCS line and a ~490 km long WAS profile along the same transect.

3.1. Multichannel Seismic Data

The MCS data were recorded with a seismic source composed of two airgun arrays with a total volume of 3,920 c.i. and air pressure of 2,000 p.s.i. deployed at 10 m depth and fired every ~37.5 m. The seismic signal was recorded in a 6 km long streamer with 480 channels 12.5 m long. This configuration provides a nominal 80-fold common-mid-point (CMP) gather data. Raw data were recorded in SEG-D format at a 2 ms sample

---

Figure 1. (a) Bathymetric map of the West Iberia margin including regional seismic profiles. Black lines correspond to WAS profiles previously acquired in the area and referred to in the text, from S to N: P2 and P1 (NEAREST survey; Sallarès et al., 2011, 2013), A-AR and B-BR (Purdy, 1975), P-B (Peirce & Barton, 1991), D1–D2 (Discovery Cruise 161; Pinheiro et al., 1992), FRAME-3 (FRAME survey, Grevemeyer et al., 2019) and WI (Davy et al., 2016). The IAM project lines (Banda & Torné, 1995): IAM5 (Afilhado et al., 2008), IAM9 (Dean et al., 2000), and IAM 11 (Ranero & Pérez-Gusinyé, 2010), and Lusigal-12 (LG12; Beslier, 1996). Map also shows the location of the FRAME-2 profile. Green line corresponds to the WAS profiles acquired during the Leg-2 and the coincident thin black line correspond to the MCS profile acquired during the Leg-1. All these profiles were acquired during the FRAME-2018 survey. Yellow and blue circles display the position of OBS and OBH along the FRAME-2 profile presented in this article. Red stars indicate ODP and DSDP sites locations. Blue line indicates the location of the J-anomaly along the margin (Srivastava, et al., 2000). Abbreviations: GO: Gorringe bank, JS: Josephine Seamount, PIAB: Paleo Iberia-Africa boundary.1.

interval. The streamer was deployed at 19–20 m depth to favor low frequency content (e.g., Williams & Pollatos, 2012). The trace length was 14.5 s for the line.

The MCS data were processed using the Globe Claritas processing software to obtain the section in Figure 5a. The processing sequence includes defining the streamer navigation and source position for the CMP binning, velocity analysis, spherical divergence correction, two-window statistical deconvolution, normal move out, near and far offset mute, stack, and post-stack finite differences time migration with a smooth velocity model based on geology. After stack, we applied an automatic gain control for amplitude balancing.

After processing, we identified key horizons and picked TT of *P* waves reflected at two different geological interfaces, namely the major intra-sedimentary unconformity and the top of the basement (TOB). We picked TT of phases reflected at each of these interfaces CMP gather images simultaneously compared to stack images for horizon visual tracking. Travel time picks were input in shot gather geometry for the inversion. We inverted every 6–8 shots, which provide a spatial sampling of 250–300 m. This sampling is lower than 400 m, which is the width of the first Fresnel zone at the depth of the first sedimentary interface (∼5 km of depth), considering a dominant frequency of 25–30 Hz. Thus, tomographic resolution is not downgraded by the decimation.

In total, we inverted 924 reflected picks for the unconformity and 1,243 for the TOB. Errors are derived from travel time uncertainty that is estimated using Zelt and Forsyth's (1994) approach. The picking uncertainty is estimated at 20–40 ms for MCS picks, based on the amplitude S/N ration between the signal within a 250 ms window before and after the selected travel time.

3.2. Wide-Angle Seismic Data

The WAS data were recorded by 35 instruments, including 17 LC2000 4 × 4 OBS from the Spanish pool, and 18 Geomar ocean bottom hydrophones (OBH). In this case, the seismic source consisted of a total of 16 airguns of the G-II model, organized in 2 symmetrical arrays with 5,200 c.i. total volume, towed behind the vessel at a depth of 15 m to enhance the low-frequency content in the source signal. The data from OBS59, OBH52, and OBH75 were corrupted, and OBS70 was not retrieved from the seafloor. The records of the other receivers have good quality, displaying seismic phases up to 100–120 km of offset after a basic data processing consisting of predictive deconvolution, 5–18 Hz bandpass filtering, and automatic gain control (Figure 2).

From East to West, the line crosses the lower continental slope of the Iberian margin, the TAP, and the J-anomaly ridge (Figure 1). The configuration of seismic phases identified in each receiver display changes characteristics along the line that occurs in five groups that we have named domains.

The record sections of OBS/H 47–110 define the first domain containing three clear seismic phases. From ∼10 to ∼30 km of offset, a phase with apparent velocity of ∼4.0–6.0 km/s is observed. We have interpreted this phase as a refraction through the post-rift sedimentary sequence and basement (Pg) (Figure 2a). From 30 to 80 km of offset OBSs records show a prominent arrival with apparent velocity of near 8.0 km/s that we interpret as a refraction within the uppermost mantle (Pn). The crossover distance between Pg and Pn is marked by a secondary arrival that we interpret as a reflection at the crust-mantle boundary (i.e., Moho), or PmP (Figure 2). This distance is similar in all receivers of this domain, indicating that crustal thickness is rather uniform there.

The OBS/H 48–54 map a second domain (Figure 1). These records display a prominent seismic phase that extends to up to 100 km of offset and have an apparent velocity of near 8.0 km/s, so we interpret it as a Pn. At near offset (<10 km), some receivers display a slower seismic phase with apparent velocity of ∼3.0–4.0 km/s that we interpret as refractions within the sedimentary cover (Ps) (Figure 2). The seismic phase configuration of these sets of receivers closely resembles that observed in exhumed mantle regions (Prada et al., 2014; Sallarès et al., 2013).

The OBS/H 55–58 records form the third group (Figure 1). These instruments show a first seismic phase with lower velocity than the second group (∼5.0 km/s) from 5 to 15–20 km offset, which we identify as a
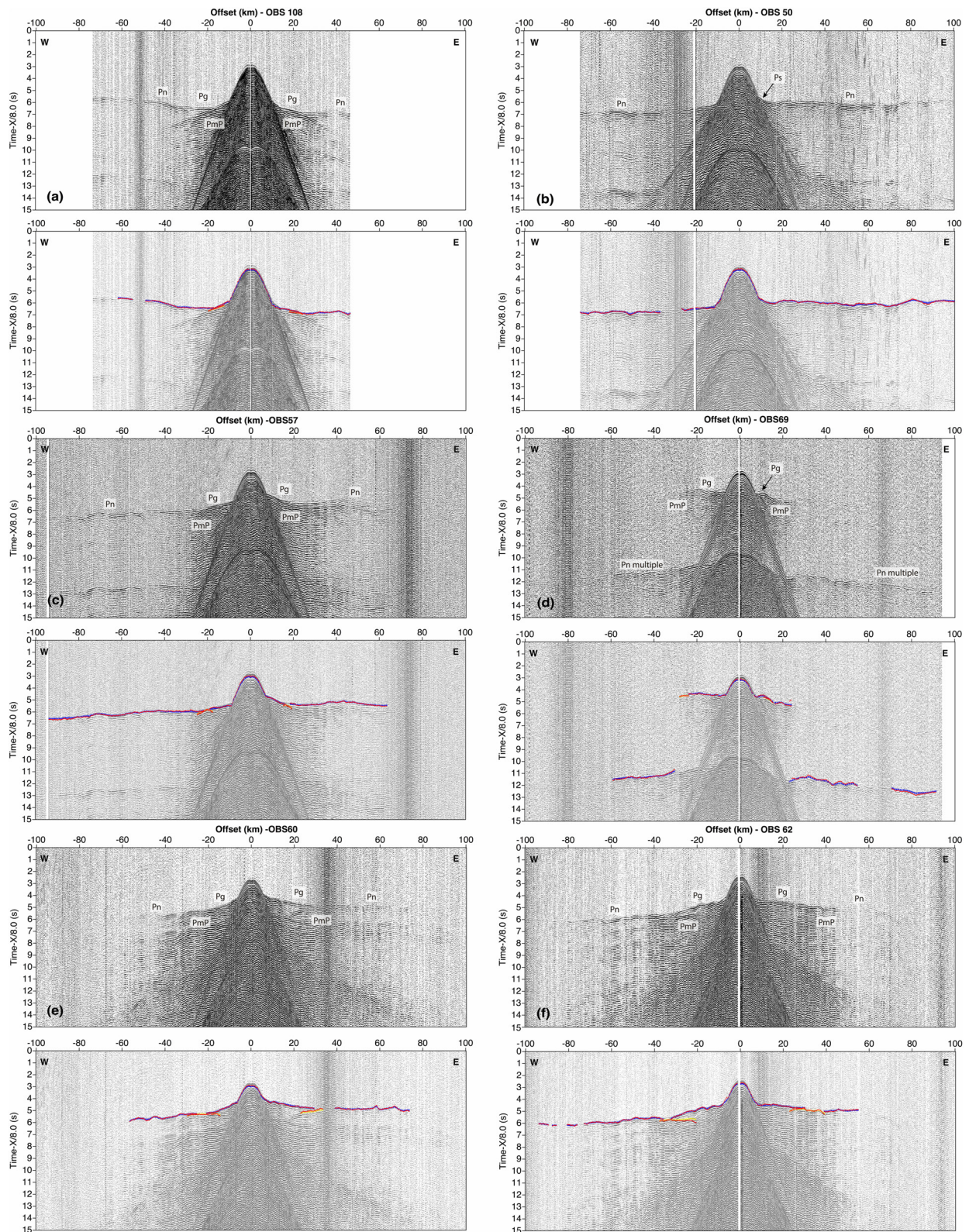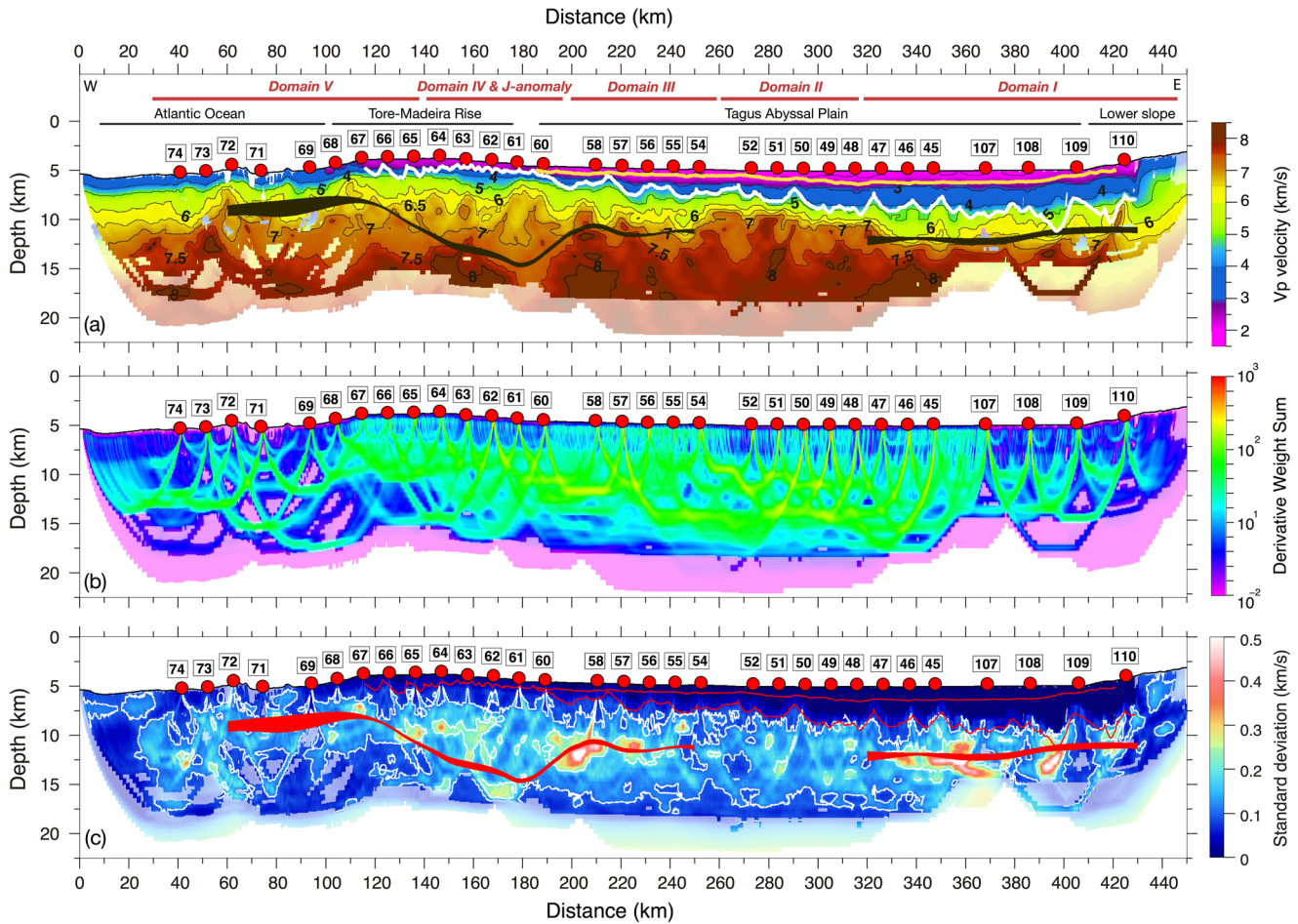
Figure 2.

Figure 3. (a) Average *V*p values from the Monte-Carlo analysis for FRAME-2 (c). The geometry of the inverted horizons is classified following a color code: in yellow the unconformity and white is the top of the basement. The width of the dark band shows the standard deviation of the depth of the Moho. (b) Average derivative weight sum (DWS) of all the inversions of tomographic model in (a). (c) Standard deviation of *V*p values of the average solution of the Monte-Carlo analysis for profile FRAME-2. The width of the red band shows the standard deviation of the depth of the inverted horizons: unconformity, top of the basement and for the Moho. Red circles display the receiver location, OBS/OBH.

Pg. Between 30 and 90 km of offset, a prominent phase with apparent velocity of 8.0 km/s is observed and interpreted as Pn. Finally, PmP phases are observed at a crossover distance between Pg and Pn of 3–5 km.

The OBS/H 60 to 64 are the fourth group. Here, Pg phases are faster than in the previous domain, with apparent exceeding 6.0 km/s between 5 and 30–40 km of offset, indicating a thicker and faster crust than in the previous domain. At offsets larger than 40 km, seismic records show a prominent Pn phase with apparent velocity of ∼8 km/s (Figure 2c). PmP reflections are also identified at the crossover distance between the two refracted phases.

The OBS/H from 65–74 groups in the fifth domain. After the direct wave, we interpreted Pg phases from ∼5 to 20 km offset, with apparent velocities of 6.0–6.5 km/s. Pn phases were identified in most receivers up to 70–80 km, with apparent velocity of ∼7.5–8.0 km/s. In some receivers, Pn phases were better observed and picked at the seafloor multiple than at the primary arrivals, possibly indicating the lack of thick water-saturated sediments and a shallow basement (Meléndez et al., 2014; Figure 2). PmP phases are interpreted at

Figure 2. Examples of wide-angle seismic data recorded at OBS/H during the FRAME survey. Record sections correspond to (a) OBS108 from Domain I, (b) OBS50 from Domain II, (c) OBS57 from Domain III, (d) OBS69 from Domain V and (e and f) OBS60-OBS62 from Domain IV. The interpretation of the seismic phases picked for the inversion is shown in the top panels. The same record with the synthetic (red circles) and observed travel times (colored vertical bars) is shown in the lower panel. Blue bars correspond to picked refracted phases (Pg and Pn), while orange and yellow correspond to continental and oceanic Moho reflections (PmP), respectively.

the crossover distance between Pg and Pn. The amplitude of this secondary phase is fainter than in the rest of domains, hampering their identification. This indicates a weaker impedance contrast between the crust and mantle than in the other domains.

In total, we manually picked 3,363 Pg, 9,171 Pn, and 1,782 PmPs arrival times. In some cases were the signal-to-noise ratio is higher, we picked TT from the multiple instead of the primary phase (e.g., OBS60 in Figure 2). This allowed to substantially increase the number of picks at far offsets.

OBS records present a smaller signal-to-noise ratio than the MCS shot gathers. The corresponding WAS picking uncertainty is therefore larger, of 40–100 ms following the same criterion as for the MCS picks (i.e., Zelt & Forsyth, 1994).

4. Methods

4.1. Joint Refraction and Reflection Travel-Time Inversion of WAS and MCS Data

We have built the final *V*p model following a two-step strategy. In the first step, we used a layer stripping strategy, explained in detail below. This approach produces a joint *V*p model that fits the travel times accurately. This model provides an accurate starting point for the next step. In the second step, we performed an uncertainty analysis (explained in Section 4.2) of the velocities of the crust and mantle. This analysis consists of a series of random perturbations of the travel times and initial model parameters within a pre-defined range. From all the fits to those pairs of data and models, we computed an average *V*p model and uncertainty and used them to analyze the *V*p-depth structure of each domain to guide our petrological interpretations.

To invert for *V*p as well as the depth of the different interfaces, we used a modified version of the joint refraction and reflection TT inversion code *tomo2d* (Begović, 2020; Korenaga et al., 2000; Meléndez et al., 2015), which allows combining MCS and WAS TT in the inversion. The initial velocity model is parametrized as a 460 km wide mesh hanging from the seafloor, with constant node spacing of 90 m in the horizontal direction, and increasing node distance with depth, from 90 m at the surface to 500 m at the bottom of the model. The reflector is set as a floating interface with a constant node spacing of 90 m. Regularization parameters including smoothing constrains are set as horizontal and vertical correlation lengths (see Table S2 in Supporting Information S1).

We followed a layer-stripping strategy to build our model layer by layer by inversion but allowing to incorporate *V*p steps between the different seismic interfaces. In this case, the inversion process included four layer-stripping steps (see Supporting Information S1).

In the first step, we inverted for the geometry of the unconformity inside the sediment layer and the overlying *V*p structure using TT from MCS reflections alone (Figure S1 in Supporting Information S1). The output of this first inversion is set as input for the following step, and the area covered by the rays during the first step is overdamped to prevent the following step to excessively modify these velocities. In addition, we impose a velocity jump beneath the resolved reflector to force the inversion to resolve the velocity contrast between both layers. This process is repeated at each step to account also for the vertical *V*p contrasts. Hence, in the second step, we inverted for the geometry of the TOB and the *V*p of the rest of the post-rift sedimentary unit. During this second step, we use TT of MCS reflections at the TOB (Figure S2 in Supporting Information S1).

We used exclusively TT from WAS data to invert for the *V*p and geometry of the underlying layers (i.e., basement and uppermost mantle). Thus, in the third step included Pg, Pn phases and PmP phases to resolve the velocity structure of the crust, mantle, and the geometry of the Moho (Figure S3 in Supporting Information S1). Including Pn phases in this step allows increasing the ray coverage, and thus, the amount of information at crustal levels. In addition, we have refined the Moho geometry between OBS 58 and 60 as important misfits in PmP arrivals was observed. Lowering the reflector correlation length from 4 to 2 km allowed to better fit PmP TT from these receivers and retrieving finer details of the Moho relief. We used the output of the third step as input for this Moho refinement (Figure S4 in Supporting Information S1).

Finally, in the last step, we inverted for Pg, PmP, and Pn phases using the velocity model obtained in the previous step but imposing a velocity step across the Moho to account for the velocity contrast of this interface and invert for mantle Vp (Figure S5 in Supporting Information S1).

The final model in Figure S6b in Supporting Information S1 has an overall root mean square (RMS) residual of 55 ms (see Table S1 in Supporting Information S1 for the RMS values at each layer-stripping step). The averaged derivative weight sum from all the layer-stripping steps, which represents the overall ray coverage of the tomographic model, is also shown in Figure S6b in Supporting Information S1.

4.2. Uncertainty and Resolution Analysis

The range of uncertainty of crustal Vp and the depth of the inverted Moho was assessed by performing a Monte Carlo-like analysis. The good agreement between the location of the inverted TOB and the observed TOB along the MCS section indicates that the sedimentary structure is well constrained. Thus, we considered this section of the model resolved and fixed during each Monte-Carlo realization in the TAP. To evaluate the Vp uncertainty of the crystalline crust, the upper mantle, and the Moho interface we have created 500 realizations each of them consisting of a 1D velocity model, a Moho interface and a set of TT with added random noise. The 1D velocity models were created by randomly varying ±10% velocities of the reference initial model in Figure S9a in Supporting Information S1. The Moho interface was generated by randomly applying a ±3 km static shift to the final Moho in the preferred model in Figure S8 in Supporting Information S1. The random Gaussian noise added to each travel time is based on the picking uncertainty, which ranges between 30 and 90 ms.

From the 500 realizations, only 336 converged below 70 ms. Those realizations that did not converge beneath this threshold correspond to models in which the Moho interface was randomly generated shallower than the average (i.e., the first final Moho, Figure S6 in Supporting Information S1). Based on Tarantola (1987), when the initial models (i.e., Vp and reflector depth ranges) cover all the regions of non-null probability within the space of possible parameters, and the data sets (i.e., picking times) cover that of the actual picking errors, the average of all the realizations corresponds to the most probable solution so that the final standard deviation is a statistical measure of the model parameters uncertainty.

We consider well-resolved areas with the following values:

$$\mathrm{DWS} \geq \overline{\mathrm{DWS}} - \sigma_{\mathrm{DWS}}$$

where DWS is derivative weight sum, $\overline{\mathrm{DWS}}$ is the average value of the derivative weight sum and σ_{DWS} the standard deviation of the DWS.

Thus, taking the final standard deviation as a proxy for parameters uncertainty and those areas of the model with an acceptable ray coverage, the model shows Vp uncertainties between ±0.1 and ±0.2 km/s, and Moho depth uncertainties between ±0.1 and ±1 km (Figure 3c). Counterintuitively, the deepest regions of the model, where ray coverage is limited (15–17 km of depth in Figure 3c), also exhibit low uncertainties (<±0.1 km/s). While this could be related to the fact that mantle velocities are rather homogeneous laterally at these depths, the checkerboard analysis presented in Figure S11b in Supporting Information S1 shows that at those depths the horizontal resolution is several tens of km and thus Vp is averaged over large regions. Localized high Vp uncertainties (i.e., >±0.3 km/s) in regions of the model with acceptable ray coverage are associated with sharp velocity contrast at the Moho interface.

We have assessed the resolution of the tomographic model by means of a checkerboard test (Figure S9 in Supporting Information S1). We tested the sensitivity of our model to a 10 × 10 km checkerboard anomaly size. We added this anomaly pattern to the final model in Figure 3a, calculated synthetic TT, and added random Gaussian noise to each TT, with a standard deviation based on pick uncertainty. After inverting the synthetic data set using the final model in Figure 3a as starting model, we show that the anomaly patter is satisfactorily retrieved along the entire model up to 12 km of depth, with some smearing occurring along the edges of the model. This indicates that our model is sensitive to lateral crustal velocity variations ≥10 km wide.
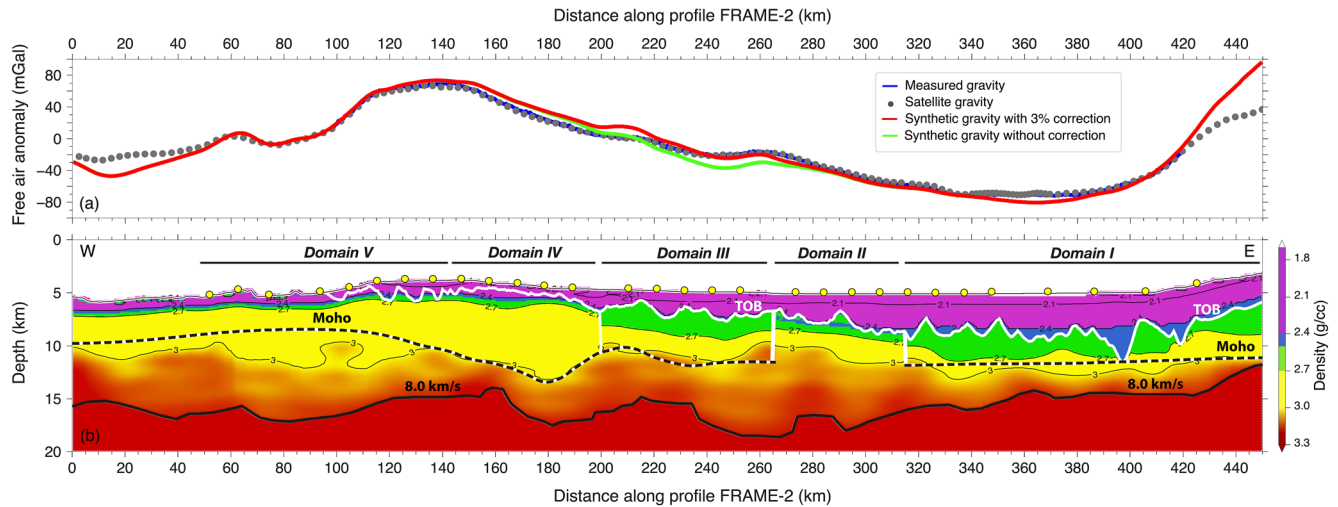
Figure 4. (a) Observed free-air gravity anomaly (blue line) recorded during the FRAME survey and gravity anomaly measured from satellite (Sandwell et al., 2014). Red line corresponds to the gravity anomaly calculated from the density model obtained by using Hamilton's (1978) relationship for the sediment layer, Christensen and Mooney's (1995) relationship for continental crust in Domains I and III, Carlson and Herrick's (1990) relationship for oceanic crust in Domains IV and V, and Carlson and Miller's (2003) conversion law for partially serpentinized peridotites in Domain II. Vp-derived density in Domain III is increased by 3% to reflect magmatic intrusions. The RMS residual is 8.39 mGal. (b) Velocity-derived density model corresponding to the best fit (red band). Yellow circles show the location of the OBS and OBH.

4.3. Gravity Modeling

To test our interpretation concerning the petrological nature of the basement, we have performed gravity modeling using the Vp model in Figure 3a as a reference. To do so, we have converted Vp into density (ρ) using Vp$-\rho$ relationships corresponding to the suit of possible petrological affinities found along rifted margins (i.e., continental, exhumed mantle, and oceanic). For the post-rift unit, we used Hamilton's (1978) Vp$-\rho$ relationship, whereas for the basement we used three different relationships. We applied Christensen and Mooney's (1995) Vp$-\rho$ relationship for rocks interpreted as continental (Domain I and III), Carlson and Herrick's (1990) conversion law for oceanic crustal rocks (Domains IV and V), and Carlson and Miller (2003)'s for partially serpentinized peridotites in Domain II. For Vp > 8.0 km/s, we assumed a constant mantle density of 3.3 g cm³. Since FRAME-2 profile is ~450 km long across from continental to oceanic lithosphere it contains long wavelength information from density contrasts deeper than the crust. We assumed an oceanic age 120 Ma old with a 120 km thick lithosphere along Domains IV and V (Fernàndez et al., 2004) and 100 km thick continental lithosphere eastwards for Domains I-III.

The resulting gravity response of the density model shows a good fit with the observed gravity anomaly, with an RMS misfit of 8.3 mGal (Figure 4). The largest misfits occur at the limits of the model due to edge effects. The larger misfit occurs in Domain III, between 200 and 220 km of the profile. Here, we increased density by 3% to take into account the influence and higher density of potential magmatic intrusions.

5. Results

The tomographic model in Figure 3a shows the Vp structure of the post-rift sedimentary sequence, the basement, and the uppermost mantle together with the geometry of an intra-sediment unconformity, the TOB, and the Moho, under the TAP and the Madeira-Tore rise. We jointly interpret the tectonic structure and the Vp distribution by overlaying the two-way time-converted Vp model on the MCS section (Figure 5).

The sediment infill has a Vp varying from ~1.8 km/s at the seafloor to ~4.0–4.5 km/s above the TOB, and it can be divided between km 180 and 450 along the model in two units separated by a regional unconformity. From east to west, the upper unit thickens toward the TAP, where it is thickest (1.5 km thick in Figure 3), and thins oceanwards, merging with the TOB at ~180 km of profile distance (Figure 5). The lower sedimentary unit seismic velocity increases from ~2.5 km/s beneath the unconformity to 4.5 km/s at the TOB (Figure 5). Both units display dominantly sub-horizontal layering, indicating post-rift deposition, although
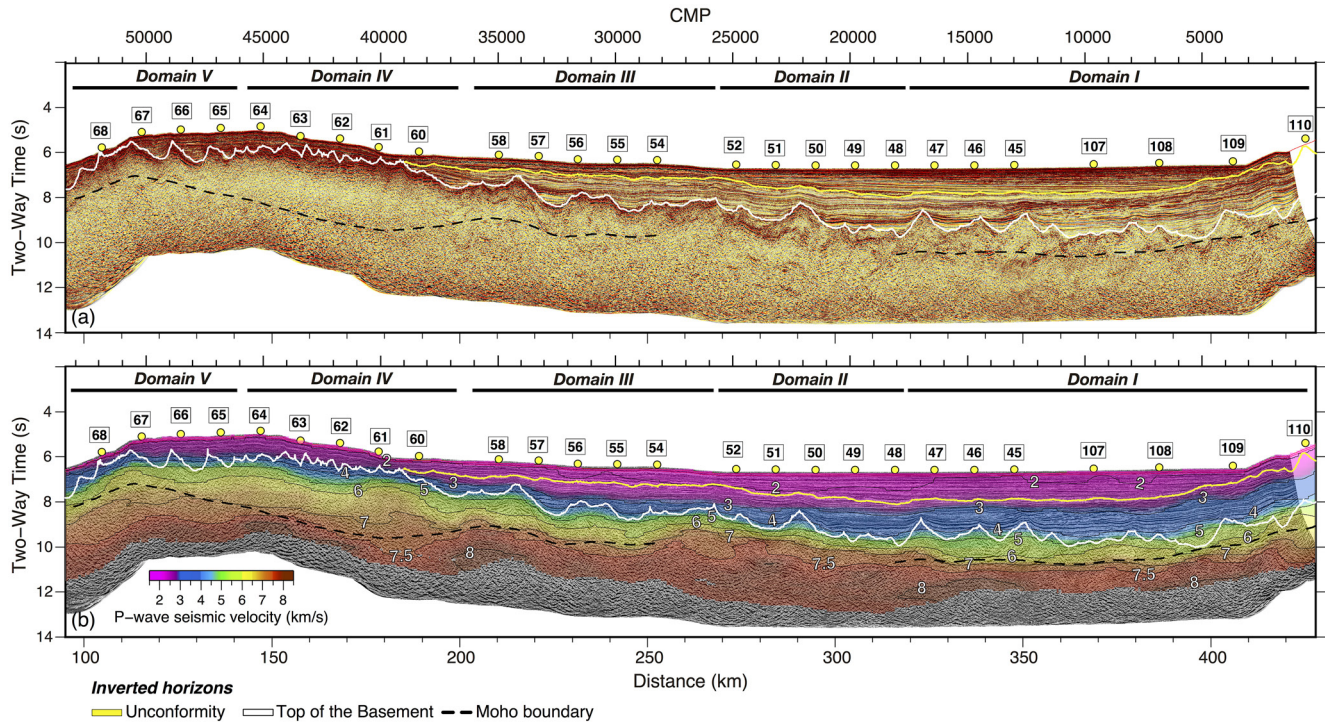
Figure 5. (a) Time-migrated MCS line overlaid with geometry of the inverted horizons by TT tomography (yellow line for the unconformity, white line for the top of the basement and dashed black line for the Moho boundary). (b) MCS image of the profile overlaid by the 2D-wave Vp average model in panel (a) converted to TWT. The inverted horizons from Figure 3a are also displayed in this figure. Yellow circles show the OBS/OBH location.

locally fan-like shape infill resting on the TOB occurs indicating syn-rift deposition (Figure 5a). The lower unit is tilted oceanwards under the lower continental slope. Similar deformation in other parts of the margin is attributed to early Tertiary contractional deformation (Afilhado et al., 2008). From km 180 to 155 the TOB shallows and is covered by the thinnest sediment along the profile. Localized thick sedimentary packages are confined inside 1–2 km deep, 5 km wide grabens (e.g., beneath OBS 67-66 in Figure 5). The reflectivity of this sediment unit is brighter than that along the TAP (Figure 5), possibly indicating the presence of sediment-interbedded igneous material. Overall, the inverted geometry of the TOB agrees with the observed morphology of the TOB imaged on the MCS section (Figure 5a). This supports that the overlying velocity structure is well resolved.

Lateral and vertical changes of Vp in the basement, and in particular the location of abrupt lateral velocity variations and crustal thickness variations support the definition of five different domains, which were already indicated above by the distinctly different character of seismic arrivals in record sections (I, II, III, IV, V; Figure 3a).

Domain I extends from km ~320 to 450 along the profile (Figure 3a). In this segment, Vp increases with depth from ~5.0 km/s to 6.0 km/s just above the Moho, which is sub-horizontal along ~100 km at ~10 km depth. The inverted topography of the TOB is highly irregular, with relief ranging from a few hundred meters to ~4 km, implying that there is extremely thin to no crustal basement in portions of the profile (i.e., ~400 km of profile distance Figures 3a and 5). The velocity contrast at the Moho is with ≤1.5 km/s rather small, because the uppermost mantle Vp is only ~7 km/s at the Moho, increasing to 8 km/s ~5 km underneath. The WAS Moho coincides with discontinuous sub-horizontal high-amplitude low-frequency reflections in the MCS section at 9–10 s TWT (Figure 5).

Domain II extends from km 250 to 320 of the model (Figure 3a). Here, Vp increases abruptly from ~4.5– 5.0 km/s at the TOB to ~7.0 km/s ~2 km underneath, and more gradually to 8 km/s at ~8–9 km into the basement (Figures 3a and 5). Thus, the vertical Vp gradient in the upper ~2 km of the basement is >1s^{-1}, two times larger than in Domain I. Domain II is also characterized by the lack of a Moho-like reflection

in the OBS recordings. Similarly, the MCS section does not display laterally continuous high-amplitude reflections where Vp $<\sim$7 km/s that might indicate a base-of-the-crust boundary. The MCS image contains several contains several gentle dipping discontinuous bright reflections at 2 s TWT into the basement where Vp is 7.5–8.0 km/s (Figure 5).

Domain III extends from km ~200 to 250 (Figure 3a). Its base is defined by clear PmP reflections and clearly imaged reflections coinciding with the inverted Moho (Figure 4). Vp increases from 5.0 km/s at the TOB, to 6.5–7.2 km/s in the lowermost crust, where is slightly higher than in Domain I. The Vp gradient is ~0.5 s^{-1}, which is half of that of Domain II. The crustal thickness along this domain is of only 4.5–5.0 km. The upper mantle Vp increases from 7.5 km/s at the Moho to 8.0 km/s ~7 km underneath. The uppermost mantle Vp of this domain is faster and laterally more homogeneous than in Domain I.

Domain IV extends from km 140 to 200, displaying the largest lateral crustal thickness variations and the smoothest TOB (Figures 3 and 4). The inverted Moho delineates a basement thickening, reaching 8–9 km, near the domain center. The basement has a 2-gradient vertical Vp structure. The Vp increases with depth from ~4.5 to 6.5 km/s in the upper 3 km with 0.6 s-1 gradient, and from 6.0 km/s to 7.0 km/s in lower crust. However, the thickest basement sector has lower crustal Vp 6.5–7.2 km/s. The Moho is well defined by PmP arrivals, but coincident near-vertical reflections at are visible at few locations (e.g., beneath OBS62 at 9 s TWT in Figure 5). The mantle Vp is 7.5–8 km/s, similar to Domain III but higher than Domain I.

Domain V extends from km ~30 to 140 (Figure 3a). From km 0 to ~30, the Vp is poorly constrained and cannot be unequivocally considered as part of Domain V. Moho is constrained by PmP phases (Figure 3), which coincide with scattered short reflections in seismic images (Figure 4). Domain V basement thins oceanward from 5 km thickness at km 140–3 km thickness at km ~50. Basement thinning is accompanied by comparatively large tilted-fault blocks (Figure 4). The vertical basement Vp gradient is laterally heterogeneous. Low Vp gradient varies between 5.0 and 6.0 km/s from TOB to mower crust (i.e., under OBS69), while strong gradient occurs at localized shallow high Vp of 7.0–7.2 km/s (i.e., under OBS 72). The uppermost 5–6 km of the mantle displays the slowest Vp along the model, ranging between 6.5 and 7.5 km/s, increasing progressively to 8.0 km/s at ~10 km into the mantle.

6. Discussion

6.1. Basement Affinity of the Geological Domains

We interpret the petrological affinity of basement domains based on their Vp structure and imaged structures. We compared the Vp-depth structure of each domain with compilations of Vp-depth profiles for continental crust (Christensen & Mooney, 1995), thinned continental crust (Prada et al., 2015), exhumed mantle (Prada et al., 2014; Sallarès et al., 2013), oceanic crust (Grevemeyer, Ranero, & Ivandic, 2018), and oceanic crust in regions with ultraslow spreading rates (Grevemeyer, Hayman, et al., 2018). We selected our Vp-depth profiles starting at the 4.5 km/s contour, which along most of the transect is close to the TOB. We chose 4.5 km/s to try to avoid Vp uncertainty associated to locations with the roughest TOB where Vp may locally be higher due to low model resolution or lower perhaps related to high rock fracturing. The comparison supports the presence of five petrological domains along the model (Figure 6). The petrological interpretation has been used to calculate density from empirical Vp-ρ relationships that explain shipborne gravity data (Figure 4) and further supports our definition of domains.

6.1.1. Domain I of Continental Crust

The Vp-depth distribution in Domain I with maximum values of ~6.5 km/s at the lower crust overlap with the reference of ultra-thin continental crust (Figure 6). The comparatively rough TOB is underlain by a smooth Moho geometry so that the basement displays large lateral changes in thickness that we interpret as fault blocks (Figure 3). Fault blocks were cut and tilted by seaward-dipping normal faults forming their west flanks (Figure 5). The continental nature of this domain is also supported by Vp$-\rho$ relationship explaining the gravity anomaly (Figure 4).

The uppermost ~4–5 km of mantle have Vp < 7.5 km/s which is anomalously low. In the SW and West Iberian margin, mantle Vp < 8.0 km/s has been found in areas of exhumed mantle, including the TAP (Pinheiro et al., 1992; Sallarès et al., 2013). Under domain I, the low mantle Vp supports mantle serpentinization
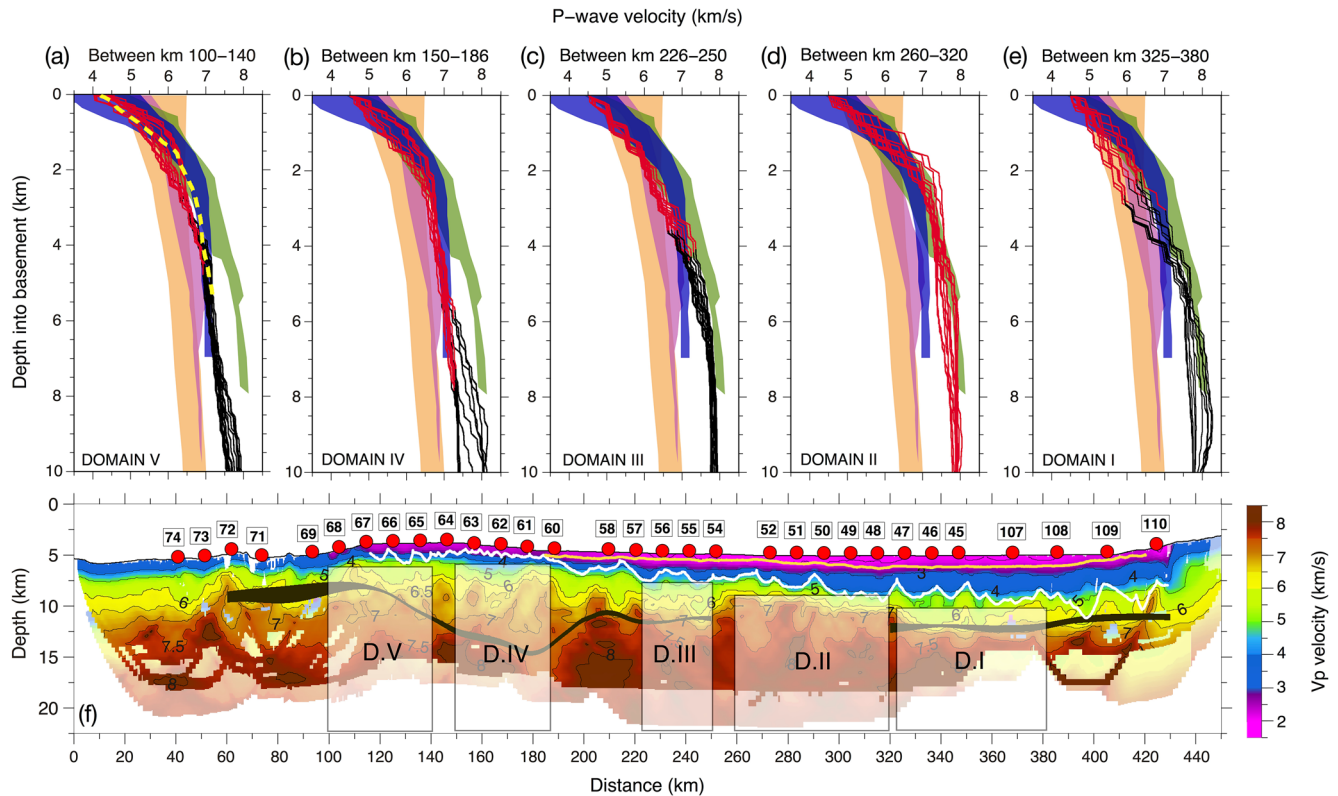
Figure 6. (a–e) Visual comparison between five reference models and the average vertical velocity structure of the 5 regions identified in the tomographic model (see model below, Figure 6f). The red profiles represent 1D profiles from each domain. The 1D *P* wave velocity depth references are displayed following the next color code: oceanic crust (from Grevemeyer, Ranero, & Ivandic, 2018) in blue, continental ultrathin crust or CUT (from Prada et al., 2015) in violet, continental crust (modified from Christensen & Mooney, 1995) in orange, and dashed yellow line for ultra-slow spreading magmatic domains (Grevemeyer, Hayman, et al., 2018). The exhumed mantle reference includes 1D *P* wave velocity depth profiles from the Gulf of Cadiz (Sallarès et al., 2013) and from the Tyrrhenian basin (Prada et al., 2014) in green. (f) Tomographic model showing the region from which 1D velocity-depth profiles are extracted in each domain.

under the continental crust, with lateral variations possibly indicating heterogeneous distribution of alteration. Low upper mantle *V*p under continental fault blocks has also been described in the Deep Galicia Margin and the Porcupine Basin, where lateral changes in *V*p appear related to deep faulting causing locally enhanced alteration (Bayrakci et al., 2016; Prada et al., 2017).

6.1.2. Domain II of Exhumed Mantle

Domain II steep *V*p-depth profiles overlap the envelop of serpentinized mantle *V*p, which together with the lack of Moho boundary in both MCS and WAS records, support that the basement is made of exhumed mantle rocks. The presence of exhumed mantle along this domain is further supported by gravity modeling (Figure 4). Although low resolution WAS data along the parallel IAM-5 line did not constrain exhumed mantle (Afilhado et al., 2008), previous low-resolution data and a modern WAS line in Tagus and HAPs (Pinheiro et al., 1992; Rovere et al., 2004; Sallarès et al., 2013) determined exhumed-mantle *V*p structure (Figure 1).

Domain II contains numerous internal basement reflections in the near-vertical images (Figure 5). There are three sets of sub-horizontal reflections underneath the TOB, one at 0.5 s TWT, a second at ~2 s TWT and a third set at ~3 s TWT (Figure 5a). Their interpretation without a detailed *V*p model is speculative. The TOB of the *V*p model maps well the corresponding boundary in the reflection image (Figure 5a). Thus, the shallowest reflections occur in the sector of the steepest *V*p vertical gradient, from 4.5 to 6.5–7.0 km/s. Their structure and lateral inter-relations are complex, and they are roughly sub-parallel to the TOB. They might represent serpentinization fronts, as interpreted for similar reflections on line IAM-9 in the IAP (Dean et al., 2000). Alternatively, they could be ~1.5–2.0 km thick slivers of continental rocks resting on exhumed mantle, representing rafted tectonic blocks. The second and third sets at ~2 and 3 s TWT underneath the

TOB respectively, occur in a broad region with 7 > Vp < 8 km/s, supporting that they are within partially serpentinized mantle.

In the absence of detailed Vp information, which is the case for the majority of seismic lines published from rifted margins, any of the two sets could speculatively be interpreted as Moho or lower crust reflections. Unless there is low-uncertainty Vp-depth information, there is no quantitative approach to test either the nature of the domains or the origin of the seismic boundaries. Although potential field data are often analyzed in an attempt to overcome this problem, they are particularly unsuited to study deep-water margins where the basement is covered in most areas by several km of sediment, so that it is too far away from shipborne sensors to provide a clear signal. Especially constraints from gravity data alone are very tenuous, because without the Vp-depth information uncertainty would be too high to discern the nature of any of these domains. This is the reason why their presence, clearly defined in the Vp-depth distribution along the model, has not being previously detected with low-resolution WAS and/or MCS data combined with potential field data modeling.

6.1.3. Domain III of Continental Crust

Domain III extends from km 200–260, and in contrast to Domain II, here the base of the crust is defined by clear PmP reflections. Basement thickness ranges from ∼4–5 km with a Vp-depth structure ranging between 4.5 km/s near the TOB to ∼6.5–7.2 km/s above Moho, and a fairly constant gradient (Figures 3 and 5). Therefore, the basement does not show the layer2-layer3-type structure of oceanic crust. This is in stark contrast with conceptual models of magma-poor margins and in particular of models for West of Iberia that assume that continental breakup is followed by mantle exhumation and subsequent well-established seafloor spreading (e.g., Sutra & Manatschal, 2012).

Domain III Vp-depth structure appears to overlap with the Vp envelop of ultra-thin continental crust (Figure 6a). The exception is the deepest ∼0.5 km of the lower crust that have Vp of 7.0–7.2 km/s, which is slightly high compared to the ultra-thin crust of other magma-poor margins (Prada et al., 2015) and to Domain I. The 7.0–7.2 km/s Vp range is typical of the gabbro of the lowermost part of oceanic layer 3 (Grevemeyer, Ranero, & Ivandic, 2018), which may indicate that Domain III is stretched continental crust that was intruded by mafic melts at low crustal levels. A 3% increase of the velocity-derived density of Domain II (estimated from empirical relationships; Christensen & Mooney, 1995), fits better the observed gravity anomaly, further supporting a rock composition somewhat more mafic than average continental.

6.1.4. Domain IV of the First Oceanic Crust

Domain IV extends from km ∼140 to 200 across the eastern flank of the Madeira Tore Rise and includes the structure causing the J-magnetic anomaly (Figure 3). The J-magnetic anomaly is attributed to oceanic crust (Srivastava, et al., 2000) or to synrift magmatism (Bronner et al., 2011; Nirrengarten et al., 2018). In TAP, the J-magnetic anomaly is centered at a ∼20 km wide segment with ∼8–9 thick basement (Figure 3a) and hence much thinner than the J-magnetic anomaly basement in the American plate of the Central Atlantic where crust is ∼12 km thick (Tucholke & Ludwig, 1982).

Domain IV has both, the most variable basement thickness, ranging from ∼6 to 9 km, and the smoothest TOB relief along the transect. A ∼20 km wide segment is 7–9 thick, which is 1–3 km thicker than typical oceanic crust (Grevemeyer, Ranero, & Ivandic, 2018). Most of Domain IV basement has a two-layer seismic structure resembling oceanic crust, that is, a layer 2 with a steep gradient and ∼4.5 < Vp > 6.5 km/and a layer 3 with a gentle gradient. However, it is somewhat different from the seismic structure of Penrose-type oceanic crust, because layer 3–6.0 < Vp < 6.7 km/s (Figure 6). Despite those departures from a classical oceanic seismic structure, the Vp−ρ conversion assuming oceanic composition (Carlson & Herrick, 1990) produces better fit to the gravity anomaly than using continental crust density.

The oceanic origin of Domain IV is further supported by findings of a similar seismic structure in locations within oceanic plates. Similarly, lower layer 3 Vp has been described as associated with thick oceanic crust in aseismic ridges, associated with the presence of mantle melting anomalies (Korenaga & Kelemen, 2000; Sallarès et al., 2003). Layer 3 bulk Vp and igneous crustal thickness either correlate when melting is thermally controlled, or anticorrelate when controlled by mantle fertility (Korenaga et al., 2002; Sallarès et al., 2003). Domain IV thicker segment shows low layer 3 Vp indicating an anticorrelation that supports that enhanced
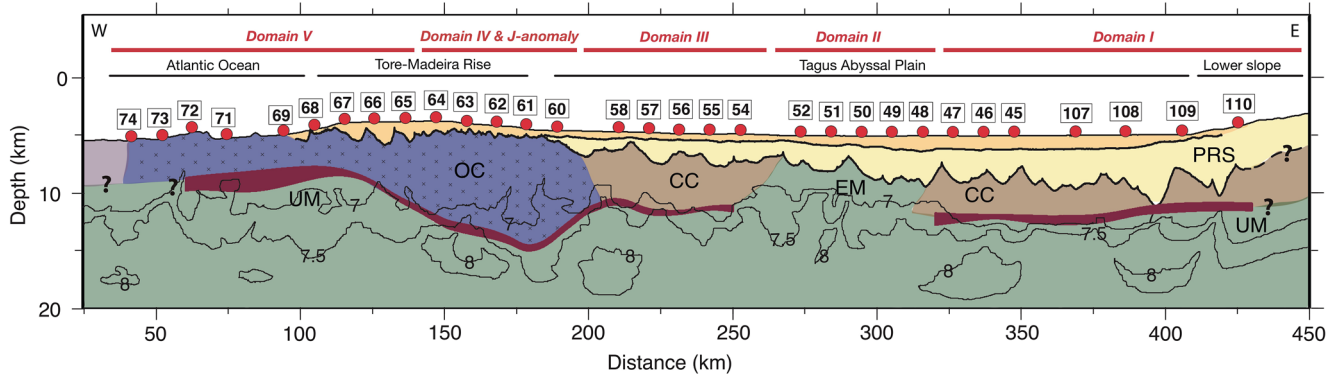
Figure 7. Interpreted cross section along the FRAME-2 profile. The interpretation is based on the 2-D *P* wave *V*p model (Figure 3a) and the corresponding basement affinity based on comparison with reference 1D *V*p-depth profiles (Figure 6). PRS: post-rift sediments, CC: continental crust, OC: oceanic crust, EM: exhumed mantle and UM: upper mantle. Isovelocity contours from 7.0, 7.5, and 8.0 km/s are also represented. Red circles show the OBS/OBH location.

melting did not result from abnormally hot mantle, but rather from either an active upwelling component and/or compositional heterogeneities in the mantle source (Sallarès et al., 2003, 2005).

Therefore, Domain IV is the first ocean crust formed during the separation of Iberia and Newfoundland, and melting was not controlled by thinning of continental lithospheric leading to synrift magmatism. Domain IV oceanic crust did not form in the region of mantle exhumation where lithospheric thinning was possibly maximum. In contrast, Domain IV oceanic crust abuts continental Domain III, conforming a configuration of crustal domains not previously described West of Iberia.

6.1.5. Domain V of the CMQZ Oceanic Crust

The *V*p-depth structure of Domain V shows an oceanic two-layer seismic structure similar to Domain IV (Figures 6 and 7). The oceanic nature is supported by gravity modeling (Figure 4). The oceanic crust formed during the Cretaceous Magnetic Quiet Zone, so that there is no direct information on spreading rate. The basement is ∼4–4.5 km thick with a laterally heterogeneous *V*p structure, particularly at middle-to-lower crustal levels. Basement *V*p ranges from <6.0 km/s (e.g., beneath OBS 69) to ∼7.0 km/s (i.e., beneath OBS 72) (Figure 6).

The TOB of Domain V is irregular compared to Domain IV, and the large blocks that appear tilted indicate normal faulting (Figure 5), although the western half of the Domain is not covered by seismic images. Alternating low *V*p sectors (e.g., beneath OBS 69) and high *V*p might indicate petrological variations or fracturing associated to faulting. Similar heterogeneous structure with high- *V*p anomalies (>7.0 km/s) occurs in Mesozoic-age oceanic crust under Coral Patch Ridge and Seine Abyssal Plain of the northern Central Atlantic (Martínez-Loriente et al., 2014), and at recently formed ultraslow spreading crust (Grevemeyer, Hayman, et al., 2018). Such variations are interpreted to arise from alternation between a magmatic spreading and moderately magmatic segments.

6.2. Rifting, Breakup, and the COT

The joint interpretation of the *V*p and density models with the tectonic structure from seismic reflection images has led to a radically new definition of the number and nature of geological domains under the TAP compared to previous studies. This new definition has important implications for rifting processes, the location, and formation of the COT and first seafloor spreading processes of the West Iberia margin during the first stages of North Atlantic opening.

Continental Domains I and III have conjugate fault structures, with overall asymmetric crustal thickness, inferred extension and fault style (Figure 7). Domain III Moho shallows as the basement thins toward the east accompanied by eastward-dipping normal faults that decrease in fault spacing and cut blocks of a decreasing size toward the basin center (Figure 5a). Domain I is characterized by westward dipping faults that

appear to cut the entire crust in a series of blocks. The Moho is mostly sub-horizontal and extends over a 100 km wide zone (Figure 5a).

The asymmetric crustal thinning and conjugate tectonic structure of Domains I and III closely resembles the structure of the Deep Galicia Margin and conjugate segment of Newfoundland (Ranero & Pérez-Gusinyé, 2010). The asymmetric tectonic configuration under TAP may be interpreted to indicate that Domain III represents a sector of the Newfoundland continental margin that was cut during opening and transferred to the West Iberia margin during the early stages of North Atlantic opening.

Our results show that the structure from the TAP margin is more complex than previously assumed. Domain II basement composed of partly serpentinized mantle peridotites, is similar toward the northern in the IAP (Dean et al., 2000; Minshull et al., 2014) and Deep Galicia Margin (Bayrakci et al., 2016; Boillot et al., 1987; Whitmarsh et al., 1996), and under the southern Tagus and HAPs (Sallarès et al., 2013). However, Domain II does not abut younger oceanic crust to the west, but limits at either side with the continental crust of Domains I and III. This structure contrasts with published interpretations of the structure along the IAP and Deep Galicia Margin, where exhumed mantle is inferred to bound oceanic lithosphere to the west (Dean et al., 2015, 2000). However, a two-layer oceanic seismic structure has not yet been shown with modern well-constraints Vp models in those two segments before the FRAME cruise. The IAP data did not map well the first ocean crust and the exhumed-mantle to oceanic crust boundary has been moved >20 km using the same data in successive analyses (Dean et al., 2000; Minshull et al., 2014) indicating the uncertainty intrinsic to the resolution of sparse data. Modern seismic data from the Deep Galicia Margin COT has not found clear ocean crust west of the outcropping peridotite ridge (Davy et al., 2016, 2015). However, in spite of the past paucity of data it has been traditionally assumed that lithospheric thinning during mantle exhumation led to, and directly preceded, the establishment of oceanic crustal accretion (e.g., Pérez-Gussinyé et al., 2006). This structural evolution did not occur in the TAP.

To explain the presence of exhumed mantle in Domain II, we propose a two-step process. A first phase of continental breakup, during which the formation of the exhumed mantle occurred, followed by a second phase where the rupture and the deformation jumped to the west forming Domain IV. Domain IV was formed by seafloor spreading with the J-magnetic anomaly being centered on 7–9 km thick oceanic crust. We thus infer that the prominent north-south striking J-magnetic anomaly delineates in the western sector of the TAP the first position of oceanic crust formed by seafloor spreading center in the north Atlantic.

6.3. Implication for Early Plate Kinematics

The newly defined configuration of basement domains cannot be explained by the classical evolutionary model of the sequential formation of domains in magma-poor margins and requires the occurrence of different rifting episodes.

6.3.1. Extensional Phase 1: From Rifting to Mantle Exhumation

We propose a geodynamic scenario in which continental rifting occurs with Domains I and III as a conjugate pair, followed by mantle exhumation forming Domain II. Rifting extended continental crust until breakup that separated Domains I and III, followed by mantle exhumation across a ∼70 km wide Domain II. The exhumed mantle domain possibly extends to the south where a similar Vp model for the basement was found in the southern Tagus and HAPs (Sallarès et al., 2013) and across the uplifted Gorrige Bank, where peridotite and gabbro were drilled (Ryan et al., 1973). However, the existence of continental crust under the TAP had not being described before, possibly due to the limited resolution of the few previous seismic studies (e.g., Afilhado et al., 2008; Mauffret et al., 1989).

We propose that the domains defined along FRAME-2 transect extend to the south to the currently Palaeo Iberia-Africa Plate Boundary (PIAB in Figure 1), but active during the Jurassic-Early Cretaceous. The fault system separated the Tagus-HAP (the uplift of Gorringe Bank had not yet occurred) from the Seine Abyssal Plain (Martínez-Loriente et al., 2014; Rovere et al., 2004; Sallarès et al., 2013). The Iberia-Africa Plate Boundary separated a magma-poor rift system with active mantle exhumation to the north from the seafloor spreading center of the Central Atlantic to the south (Figure 8).
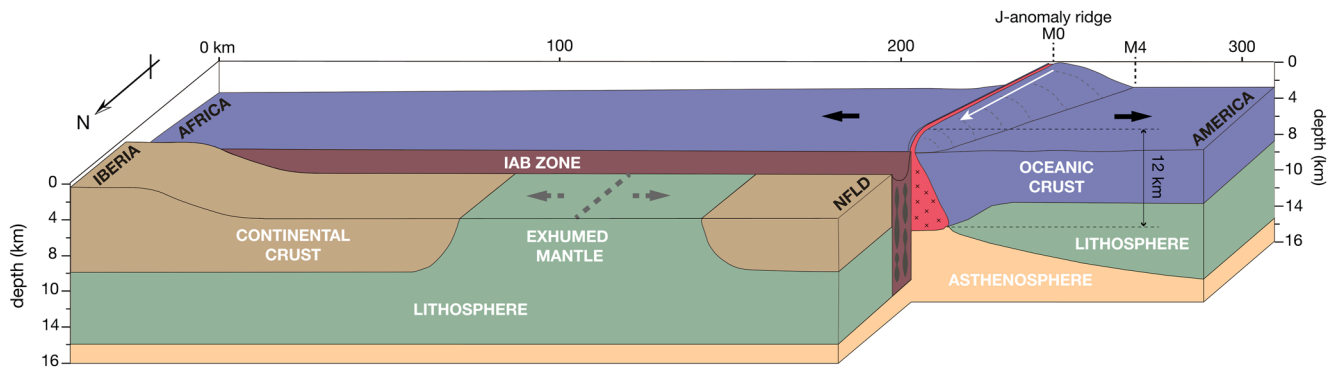
Figure 8. Conceptual cartoon of the crustal and lithospheric structure Domains I-III right before the formation of oceanic Domain IV. The magma-rich J-anomaly ridge propagation (white arrow indicates the propagation direction of the spreading center) has been blocked by the Iberia-Africa plate boundary (IAB) separating the thin spreading-center lithosphere from the West Iberia thicker plate. The reconstruction represents the structure along FRAME-2 profile with extension axis (dashed and gray line and arrows) exhuming mantle of Domain II as Iberia and Newfoundland tectonic plates were pulled apart. Vertical exaggeration ~2.5. IAB, Iberia-Africa Boundary; NFLD, Newfoundland.

The existence of two domains with continental basement under the TAP appears to imply that the extensional system in Figure 8 abruptly stopped during mantle exhumation in the Early Cretaceous, and that the locus of extension jumped to the west of Domain III. The jump of the center of extension severed a sector of the conjugate Newfoundland continental margin and transferred it to the Iberia plate, forming Domain III (Figure 7). Our scenario implies that extension in the exhumed mantle section was interrupted before initiation of seafloor spreading, in contrast to what is proposed by previous models of West Iberia margin formation (e.g., Bronner et al., 2011; Nirrengarten et al., 2018).

The exhumed-mantle domain under TAP is ~60 km wide, under IAP is >150 km wide, whereas under the Deep Galicia Margin it extends from the peridotite ridge at site 637 to the west for >50 km. However, line WI did not find a two-layer oceanic seismic structure, like in the south, and the first oceanic crust formed at the spreading center propagating north has not yet being detected (Figure 1). Thus, exhumed mantle domains do not follow the commonly assumed model where the TAP has a wider domain and the amount of mantle exhumation decreases toward the north (e.g., Nirrengarten et al., 2018).

6.3.2. Extensional Phase 2: Seafloor Spreading

The second phase of extension occurs with an intense first pulse of magmatism creating Domain IV (Figure 3). The Vp and gravity models of the structure support that Domain IV is made of thick oceanic crust formed at a well-established seafloor spreading center for the first time in the North Atlantic (Figure 7). The J-magnetic anomaly is centered above the thick sector of Domain IV. Thus, our data support that the J-magnetic anomaly is a lineation related to seafloor spreading volcanism. This finding is in contrast to numerous previous studies that interpreted the J-magnetic anomaly located north of the IAB boundary either as resulting from a magmatic pulse associated to continental breakup before seafloor spreading (Bronner et al., 2011; Olivet, 1996; Sibuet et al., 2004), or formed by multiple magmatic events that occurred both during and after formation of oceanic crust (Nirrengarten et al., 2018). A corollary to those previous interpretations was that the J-magnetic anomaly would either correspond to an isochron younger than M0 (Tucholke et al., 2007), or was not an isochron and its age changed in an undetermined fashion along its strike (Bronner et al., 2011).

The comparatively low resolution of previous studies of the basement structure have led to the proposition that the J-anomaly magmatic event formed the relief of the Madeira Tore Rise (Afilhado et al., 2008; Bronner et al., 2011). However, the thick oceanic crust of Domain IV does not occur under the shallowest topography of the Madeira-Tore Rise (Figure 1), but under the eastern slope (Figure 3). It is unclear why the ridge of the Madeira-Tore Rise is higher to the west of the thick crust, it could be due to the decrease in density of the underlaying mantle due to serpentinization as indicated by the low Vp (Figure 3), or to tectonic processes from the Cenozoic contractional reactivation of different structures along the margin or both.
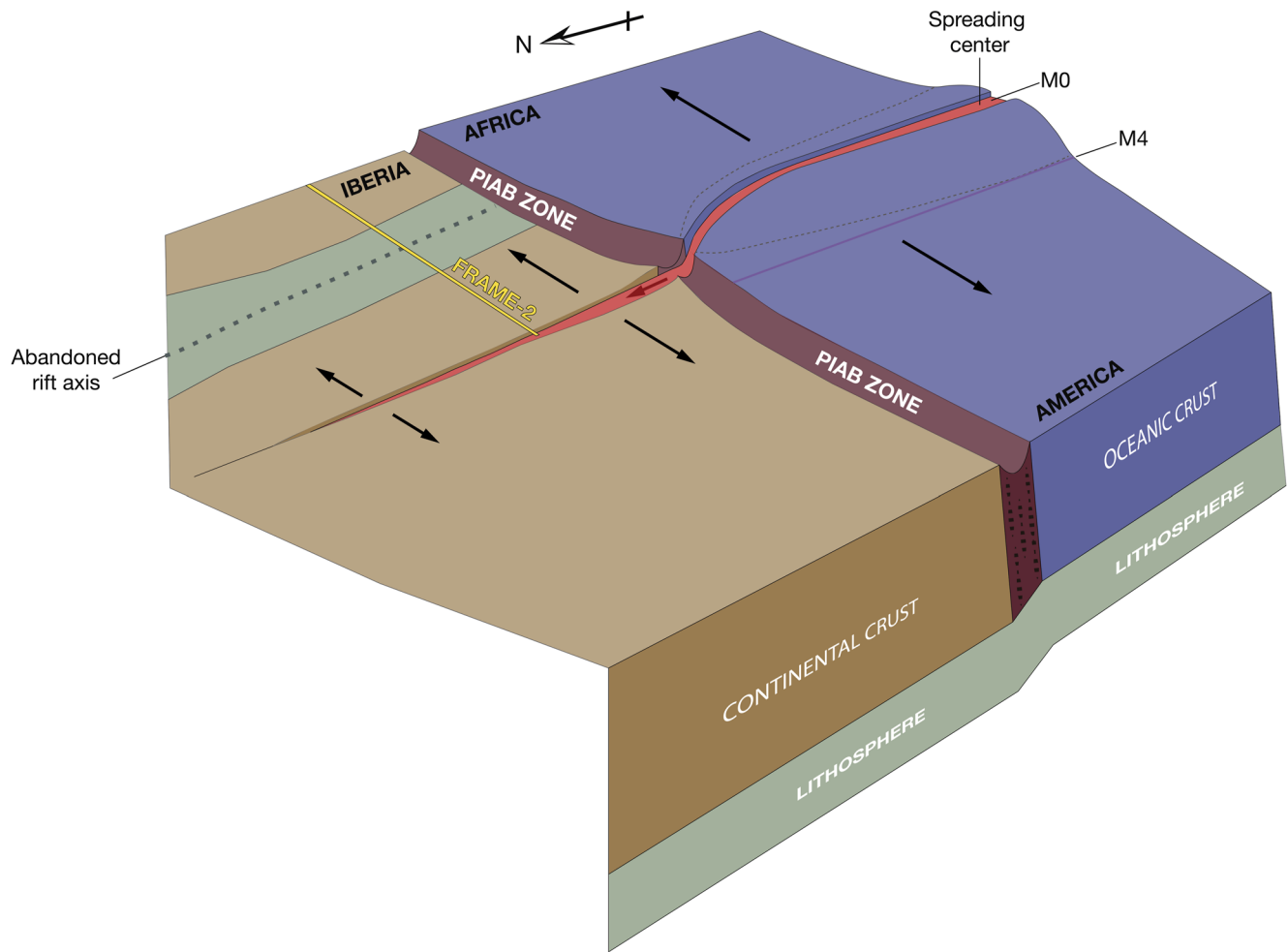
Figure 9. Conceptual cartoon of the oceanic propagation event, following the model in Figure 8, across the PIAB zone and the Tagus Abyssal Plain. The red arrow located at the spreading center represents the gravitational stress and the black arrows represent the extension direction of the tectonics plates: Africa, America, Iberia, and Newfoundland. The yellow line represents the location of FRAME-2 profile. Abbreviations: PIAB: Paleo Iberia-Africa Boundary.

Therefore, we conclude that J-magnetic anomaly across the FRAME-2 transect is a seafloor spreading lineation formed after the jump of the locus of extension that terminated mantle exhumation and that transferred continental Domain III from Newfoundland to Iberia (Figure 9). The implications are that it is possibly that the J-magnetic anomaly in the TAP is an extension of the J-magnetic anomaly within the oceanic plate of the central Atlantic south of the PIAB.

Along the northern Central Atlantic, the high-amplitude J-magnetic anomaly is interpreted as a seafloor spreading lineation. Here, the J-magnetic lineation is a continuous feature roughly parallel to older anomalies of the Mesozoic M-series and it is interpreted to contain the M4 to M0 isochrons (~126–120.95 Ma; Malinverno et al., 2012) and M4 has, at least along some of its length (Klitgord & Schouten, 1986; Rabinowitz et al., 1979; Verhoef et al., 1991). The J-magnetic anomaly occurs partly over a continuous basement ridge (Roest et al., 1992) of oceanic igneous crust ~12 km thick (Tucholke & Ludwig, 1982) that was near sea-level at least in some segments where drilling sampled reef limestone covering basalts (Tucholke & Vogt, 1979). This set of observations supports that the J-magnetic anomaly along the northern Central Atlantic corresponds to an igneous structure formed at a spreading center sector with enhanced magmatism.

We speculate that the J-anomaly magmatism may have promoted ridge propagation, a process by which a spreading segment enlarges at the expense of neighboring segments. The magma-rich TAMMAR segment of the Mid Atlantic Ridge opening at slow-intermediate rates, that is, similar to the spreading rates along the J-magnetic anomaly, currently exhibits ridge propagation characteristics (Dannowski et al., 2011). The

TAMMAR segment lengthening has led to the recent termination of a transform fault bounding spreading segments and the cessation of associated detachment faulting (Dannowski et al., 2018).

We propose that when the J-anomaly ridge initiated at M4, the magma-rich segment propagated north approaching the Iberia-Africa Boundary Zone (Figure 8). We do not have data to determine when the magma-rich ridge arrived to the plate boundary separating the Central Atlantic oceanic plate from the north Atlantic continental plate. The mid-ocean ridge migrating north may have been temporally stopped by the thicker continental lithosphere in the mantle exhumation phase or may have being able to relatively swiftly further migrate across the Iberia-Africa Boundary Zone (Figure 9). The doming caused by thicker than average melt column in the asthenosphere and melt chamber in the crust created gravitational stresses to drive propagation (Mondy et al., 2018). We envision a melt-infiltrated frontal fissure propagating across the Iberia-Africa Boundary Zone from the Central Atlantic spreading center to the north across the rifted continental lithosphere (Figure 9). The melt-rich spreading center propagating north took all deformation associated to the opening, causing cessation of mantle exhumation at Domain II, severing a sector of the continental plate of the Newfoundland margin transferred as Domain III, and terminated the differential slip across the Iberia-Africa Boundary Zone making the plate boundary inactive (PIAB, Figure 9).

The propagation of a magma-rich spreading center explains the structure of Domain IV that is the first oceanic crust of the margin with a layer2/3 seismic structure and 7–9 km thick, i.e., 2–3 km thicker than normal crust formed at similar spreading rates (Grevemeyer, Ranero, & Ivandic, 2018). The propagation also explains the presence of the continental Domain III and may explain its slightly higher lower crust Vp perhaps associated to melt intrusions in the lower continental crust. The model implies that the first oceanic crust is not related to the gradual extension and thinning of continental lithosphere during rifting and that it is not the consequence of mantle melting processes associated to gradual mantle exhumation as proposed in conceptual models for IAP and Galicia margin (e.g., Bronner et al., 2011). Furthermore, this pulse of magmatism that is ultimately responsible for breakup has no relation with mantle exhumation and serpentinization in the TAP.

The geodynamic evolution implies that the 60 km of Domain II may represent the entire width of exhumed mantle produced during rifting and that the conjugate North American margin may not necessarily have any exhumed mantle domain as often assumed (Nirrengarten et al., 2018). The propagation of the magmatically robust ridge caused a second breakup, after the continental breakup leading to mantle exhumation. The spreading center moved northward at unknown speed, so that the J-magnetic anomaly west of Iberia should be younger toward the north, but whether it represents the M0 isochron along its entire length or a longer time span is still unresolved. Enhanced melting source under the spreading center stopped after M0, and the oceanic igneous crust gradually thins from 6 to ~3 km thickness from Domain IV to Domain V, in agreement with the ultraslow spreading rates estimated for the beginning of the Cretaceous Magnetic Quiet Zone (Schettino & Turco, 2011).

7. Conclusions

A joint tomography of reflections and first arrivals in collocated streamer data and OBS records across the Tagus Abyssal Plain provides a Vp model of the crust and uppermost mantle that constrains the properties and limits of the different geological domains of the basement.

The basement has five domains differentiated in their Vp and gravity models and seismic image. Each domain has a distinct crustal geometry and Vp and density structure. From east to west, Domains I and III are made of extended continental crust. Domain II is 60 km wide made of exhumed partly serpentinized mantle. Westwards is Domain IV with a layer 2 and layer 3 type oceanic crust seismic structure. Domain IV has a 7–9 km thick sector that corresponds to the location of the J-magnetic anomaly. The igneous oceanic crust thins further west from 6 to 3 in Domain V formed during the Cretaceous Magnetic Quiet Zone possibly formed at ultraslow spreading rates.

The distribution of basement domains is at odds with evolutionary magma-poor models for the West Iberia margin where continental breakup is followed by mantle exhumation that promotes asthenospheric rise and the establishment of a stable spreading system.

In contrast, we propose after continental breakup of conjugate Domains I and III, when mantle exhumation was active West Iberia in Domain II, an independent event occurred in the Central Atlantic that would subsequently terminate continental rifting and start seafloor spreading in the North Atlantic. A magma-rich spreading center formed from M4 to M0 magnetic isochron age and propagated to the north to cut the plate boundary between Iberia and African plates. The spreading center propagation cut through a sector of the Newfoundland continental lithosphere and transferred Domain III to Iberia, and ended mantle exhumation (Domain II) as all deformation focused on the weak magma-rich system (Domain IV). The thick igneous crust sector of Domain IV generates the J-magnetic anomaly in TAP. Thus, the 3D development of the rift to drift system of West Iberia is not related to the gradual 2D evolution of the thinning of the lithosphere envision by most current conceptual models of magma-poor margins in the literature.

Data Availability Statement

Seismic and gravity data were collected by Spanish R/V Sarmiento de Gamboa in 2018. High-resolution images of the data used in this article are available in Figshare public database (https://figshare.com/articles/figure/MCS-seismic-line-interpreted_pdf/14865480 and https://figshare.com/articles/figure/OBS_H-seismic-record-sections_pdf/14865483). The bathymetric grid is freely available as a.xyz file from the website of the EMODnet (https://www.emodnet-bathymetry.eu/) and Generic Mapping Tools (Wessel & Smith, 1995) was used in the preparation of this manuscript.

References

Afilhado, A., Matias, L., Shiobara, H., Hirn, A., Mendes-Victor, L., & Shimamura, H. (2008). From unthinned continent to ocean: The deep structure of the West Iberia passive continental margin at 38°N. *Tectonophysics*, *458*(1–4), 9–50. https://doi.org/10.1016/j.tecto.2008.03.002

Banda, E., & Torné, M. (1995). Iberia Atlantic Margins Group investigates deep structure of ocean margins. *EOS, Transactions, AGU*, *76*(25), 29–29.

Bayrakci, G., Minshull, T. A., Sawyer, D. S., Reston, T. J., Klaeschen, D., Papenberg, C., et al. (2016). Fault-controlled hydration of the upper mantle during continental rifting. *Nature Geoscience*, *9*(5), 384–388. https://doi.org/10.1038/ngeo2671

Begović, S. (2020). *Structure and physical properties of the subduction plate boundary, (Ph.D. Thesis)*. Universitat de Barcelona.

Beslier, M. O. (1996). Data report: Seismic line LG12 in the Iberia Abyssal Plain. In R. B. Whitmarsh, D. S. Sawyer, A. Klaus, & D. G. Masson (Eds.), *Proceeding of Ocean Drill. Program, Sci. Results* (Vol. 149, pp. 737–739). https://doi.org/10.2973/odp.proc.sr.149.257.1996

Boillot, G., Winterer, E., & Meyer, A. (1987). Introduction, objectives, and principal results: Ocean Drilling Program Leg 103, west Galicia Margin, Proc. Ocean Drill. Program, Initial Reports.

Bronner, A., Sauter, D., Manatschal, G., Péron-Pinvidic, G., & Munschy, M. (2011). Magmatic breakup as an explanation for magnetic anomalies at magma-poor rifted margins. *Nature Geoscience*, *4*(8), 549–553. https://doi.org/10.1038/ngeo1201

Carlson, R. L., & Herrick, C. N. (1990). Densities and porosities in the oceanic crust and their variations with depth and age. *Journal of Geophysical Research: Solid Earth*, *95*(B6), 9153–9170. https://doi.org/10.1029/jb095ib06p09153

Carlson, R. L., & Miller, D. J. (2003). Mantle wedge water contents estimated from seismic velocities in partially serpentinized peridotites. *Geophysical Research Letters*, *30*(5). https://doi.org/10.1029/2002GL016600

Christensen, N., & Mooney, W. (1995). Seismic velocity structure and composition of the continental crust: A global view. *Journal of Geophysical Research: Solid Earth*, *100*(B7), 9761–9788. https://doi.org/10.1029/95JB00259

Dannowski, A., Grevemeyer, I., Phipps Morgan, J., Ranero, C. R., Maia, M., & Klein, G. (2011). Crustal structure of the propagating TAMMAR ridge segment on the Mid-Atlantic Ridge, 21.5°N. *Geochemistry, Geophysics, Geosystems*, *12*, Q07012. https://doi.org/10.1029/2011GC003534

Dannowski, A., Morgan, J. P., Grevemeyer, I., & Ranero, C. R. (2018). Enhanced mantle upwelling/melting caused segment propagation, oceanic core complex die off, and the death of a transform fault: The Mid-Atlantic Ridge at 21.5°N. *Journal of Geophysical Research: Solid Earth*, *123*, 941–956. https://doi.org/10.1002/2017JB014273

Davy, R. G., Minshull, T. A., Bayrakci, G., Bull, J. M., Klaeschen, D., Papenberg, C., et al. (2016). Continental hyperextension, mantle exhumation and thin oceanic crust at the continent-ocean transition, West Iberia: New insights from wide-angle seismic. *Journal of Geophysical Research: Solid Earth*, *121*, 3177–3199. https://doi.org/10.1002/2016JB012825

Dean, S., Sawyer, D., & Morgan, J. (2015). Galicia Bank ocean-continent transition zone: New seismic reflection constraints. *Earth and Planetary Sciences Letters*, *413*, 197–207.

Dean, S. M., Minshull, T. A., Whitmarsh, R. B., & Louden, K. E. (2000). Deep structure of the ocean-continent transition in the southern Iberia Abyssal Plain from seismic refraction profiles: The IAM-9 transect at 40°20′N. *Journal of Geophysical Research*, *105*(B3), 5859–5885. https://doi.org/10.1029/1999JB900301

Fernàndez, M., Marzán, I., & Torne, M. (2004). Lithospheric transition from the Variscan Iberian Massif to the Jurassic oceanic crust of the Central Atlantic. *Tectonophysics*, *386*, 97–115.

Grevemeyer, I., Hayman, N. W., Peirce, C., Schwardt, M., Van Avendonk, H. J., Dannowski, A., & Papenberg, C. (2018). Episodic magmatism and serpentinized mantle exhumation at an ultraslow-spreading center. *Nature Geoscience*, *11*(6), 444–448. https://doi.org/10.1038/s41561-018-0124-6

Grevemeyer, I., Ranero, C. R., & Ivandic, M. (2018). Structure of oceanic crust and serpentinization at subduction trenches. *Geosphere*, *14*(2), 395–418. https://doi.org/10.1130/GES01537.1

Grevemeyer, I., Sallares, V., Ranero, C. R., Bartolomé, R., Prada, M., Batista, L., & Neres, M. (2019). The continent-ocean transition zone in the Iberia Abyssal Plain re-visited: Seismic constraints from FRAME profile P3. In Geophysical Research Abstracts (Vol. 21).

Hamilton, E. L. (1978). Sound velocity-density relations in sea-floor sediments and rocks. *Journal of the Acoustical Society of America*, *63*, 366–377. https://doi.org/10.1121/1.381747

Klitgord, K. D., & Schouten, H. (1986). Plate kinematics of the central Atlantic. *The Geology of North America*, *1000*, 351–378.

Korenaga, J., Holbrook, W., Kent, G., Kelemen, P., Detrick, R., Larsen, H. C., et al. (2000). Crustal structure of the southeast Greenland margin from joint refraction and reflection seismic tomography. *Journal of Geophysical Research*, *105*, 21591–21614. https://doi.org/10.1029/2000jb900188

Korenaga, J., & Kelemen, P. B. (2000). Major element heterogeneity in the mantle source of the North Atlantic igneous province. *Earth and Planetary Science Letters*, *184*(1), 251–268. https://doi.org/10.1016/s0012-821x(00)00308-3

Korenaga, J., Kelemen, P. B., & Holbrook, W. S. (2002). Methods for resolving the origin of large igneous provinces from crustal seismology. *Journal of Geophysical Research*, *107*(B9), ECV 1-1-ECV 1-27. https://doi.org/10.1029/2001JB001030

Malinverno, A., Hildebrandt, J., Tominaga, M., & Channell, J. E. (2012). M-sequence geomagnetic polarity time scale (MHTC12) that steadies global spreading rates and incorporates astrochronology constraints. *Journal of Geophysical Research: Solid Earth*, *117*(B6). https://doi.org/10.1029/2012jb009260

Martínez-Loriente, S., Sallarès, V., Gràcia, E., Bartolome, R., Dañobeitia, J. J., & Zitellini, N. (2014). Seismic and gravity constraints on the nature of the basement in the Africa-Eurasia plate boundary: New insights for the geodynamic evolution of the SW Iberian margin. *Journal of Geophysical Research: Solid Earth*, *119*(1), 127–149.

Mauffret, A., Mougenot, D., Miles, P. R., & Malod, J. A. (1989). Cenozoic deformation and Mesozoic abandoned spreading center in the Tagus Abyssal-Plain (West of Portugal)—Results of a multichannel seismic survey. *Canadian Journal of Earth Sciences*, *26*(6), 1101–1123. https://doi.org/10.1139/e89-095

Meléndez, A., Korenaga, J., Sallarès, V., Miniussi, A., & Ranero, C. R. (2015). TOMO3D: 3-D joint refraction and reflection travel-time tomography parallel code for active-source seismic data—Synthetic test. *Geophysical Journal International*, *203*, 158–174. https://doi.org/10.1093/gji/ggv292

Meléndez, A., Sallarès, V., Ranero, C. R., & Kormann, J. (2014). Origin of water layer multiple phases with anomalously high amplitude in near-seafloor wide-angle seismic recordings. *Geophysical Journal International*, *196*(1), 243–252. https://doi.org/10.1093/gji/ggt391

Minshull, T., Dean, S., & Whitmarsh, R. (2014). The Peridotite Ridge province in the southern Iberia Abyssal Plain: Seismic constraints revisited. *Journal of Geophysical Research: Solid Earth*, *119*, 1580–1598. https://doi.org/10.1002/2014JB011011

Mondy, L. S., Rey, P. F., Duclaux, G., & Moresi, L. (2018). The role of asthenospheric flow during rift propagation and breakup. *Geology*, *46*, 103–106. https://doi.org/10.1130/G39674.1

Nirrengarten, M., Manatschal, G., Tugend, J., Kusznir, N., & Sauter, D. (2018). Kinematic evolution of the southern North Atlantic: Implications for the formation of hyperextended rift systems. *Tectonics*, *37*(1), 89–118. https://doi.org/10.1002/2017tc004495

Nirrengarten, M., Manatschal, G., Tugend, J., Kusznir, N. J., & Sauter, D. (2017). Nature and origin of the J-magnetic anomaly offshore Iberia-Newfoundland: Implications for plate reconstructions. *Terra Nova*, *29*(1), 20–28. https://doi.org/10.1111/ter.12240

Olivet, J.-L. (1996). La cinématique de la plaque Ibérie. *Bulletin des Centres de Recherches Exploration-Production Elf-Aquitaine*, *20*, 131–195.

Peirce, C., & Barton, P. J. (1991). Crustal structure of the Madeira-Tore Rise, Eastern North-Atlantic—Results of a DOBS wide-angle and normal incidence seismic experiment in the Josephine Seamount region. *Geophysical Journal International*, *106*(2), 357–378. https://doi.org/10.1111/j.1365-246x.1991.tb03898.x

Pérez-Gussinyé, M., Morgan, J. P., Reston, T. J., & Ranero, C. R. (2006). The rift to drift transition at non-volcanic margins: Insights from numerical modeling. *Earth and Planetary Science Letters*, *244*(1–2), 458–473. https://doi.org/10.1016/j.epsl.2006.01.059

Pérez-Gussinyé, M., Ranero, C. R., Reston, T. J., & Sawyer, D. (2003). Mechanisms of extension at nonvolcanic margins: Evidence from the Galicia interior basin, west of Iberia. *Journal of Geophysical Research: Solid Earth*, *108*(B5).

Pérez-Gussinyé, M., & Reston, T. J. (2001). Rheological evolution during extension at nonvolcanic rifted margins: Onset of serpentinization and development of detachments leading to continental breakup. *Journal of Geophysical Research: Solid Earth*, *106*(B3), 3961–3975.

Pickup, S. L. B., Whitmarsh, R. B., Fowler, C. M. R., & Reston, T. J. (1996). Insight into the nature of the ocean-continent transition off West Iberia from a deep multichannel seismic reflection profile. *Geology*, *24*(12), 1079–1082. https://doi.org/10.1130/0091-7613(1996)024<1079:iitnot>2.3.co;2

Pinheiro, L. M., Whitmarsh, R. B., & Miles, P. R. (1992). The ocean-continent boundary off the western continental margin of Iberia—II. Crustal structure in the Tagus abyssal plain. *Geophysical Journal International*, *109*(1), 106–124. https://doi.org/10.1111/j.1365-246x.1992.tb00082.x

Prada, M., Sallarès, V., Ranero, C. R., Vendrell, M. G., Grevemeyer, I., Zitellini, N., & de Franco, R. (2014). Seismic structure of the Central Tyrrhenian basin: Geophysical constraints on the nature of the main crustal domains. *Journal of Geophysical Research: Solid Earth*, *119*, 52–70. https://doi.org/10.1002/2013JB010527

Prada, M., Sallarès, V., Ranero, C. R., Vendrell, M. G., Grevemeyer, I., Zitellini, N., & de Franco, R. (2015). The complex 3-D transition from continental crust to back-arc magmatism and exhumed mantle in the Central Tyrrhenian Basin. *Geophysical Journal International*, *203*(1), 63–78. https://doi.org/10.1093/gji/ggv271

Prada, M., Watremez, L., Chen, C., O'Reilly, B. M., Minshull, T. A., Reston, T. J., et al. (2017). Crustal strain-dependent serpentinization in the Porcupine Basin, offshore Ireland. *Earth and Planetary Science Letters*, *474*, 148–159. https://doi.org/10.1016/j.epsl.2017.06.040

Purdy, G. M. (1975). The Eastern end of the Azores-Gibraltar plate boundary. *Geophysical Journal Royal Astronomical Society*, *43*, 123–150. https://doi.org/10.1111/j.1365-246x.1975.tb06206.x

Rabinowitz, P. D., Cande, S. C., & Hayes, D. E. (1979). The J-Anomaly in the Central North Atlantic Ocean. In *Initial Reports of the Deep Sea Drilling Project* (Vol. 43, pp. 879–885). U.S. Government Printing Office. https://doi.org/10.2973/dsdp.proc.43.145.1979

Ranero, C. R., & Pérez-Gusinyé, M. (2010). Sequential faulting explains the asymmetry and extension discrepancy of conjugate margins. *Nature*, *468*, 294–299. https://doi.org/10.1038/nature09520

Reston, T. J., & Morgan, J. P. (2004). Continental geotherm and the evolution of rifted margins. *Geology*, *32*, 133–136. https://doi.org/10.1130/g19999.1

Roest, W. R., Dañobeitia, J. J., Verhoef, J., & Collette, B. J. (1992). Magnetic anomalies in the Canary Basin and the Mesozoic evolution of the Central North Atlantic. *Marine Geophysical Researches*, *14*, 1–24. https://doi.org/10.1007/bf01674063

Rovere, M., Ranero, C. R., Sartori, R., Torelli, L., & Zitellini, N. (2004). Seismic images and magnetic signature of the Late Jurassic to Early Cretaceous Africa-Eurasia plate boundary off SW Iberia. *Geophysical Journal International*, *158*, 554–568. https://doi.org/10.1111/j.1365-246x.2004.02339.x

Russell, S. M., & Whitmarsh, R. B. (2003). Magmatism at the west Iberia non-volcanic rifted continental margin: Evidence from analyses of magnetic anomalies. *Geophysical Journal International*, *154*(3), 706–730. https://doi.org/10.1046/j.1365-246x.2003.01999.x

Ryan, W. B. R., Hsü, K. J., Cita, M. B., Dumitrica, P., Lort, J., Maync, W., et al. (1973). Site 120. In A. G. Kaneps (Ed.), *Initial Reports of the Deep-Sea Drilling Project, JOIDES* (Vol. 13, pp. 19–41). U.S. Government Printing Office. https://doi.org/10.2973/dsdp.proc.13.102.1973

Sallarès, V., Charvis, P., Flueh, E. R., & Bialas, J. (2003). Seismic structure of Cocos and Malpelo Volcanic Ridges and implications for hot spot-ridge interaction. *Journal of Geophysical Research: Solid Earth*, *108*(B12).

Sallarès, V., Charvis, P., Flueh, E. R., & Bialas, J., & the SALIERI Scientific Party. (2005). Seismic structure of the Carnegie ridge and the nature of the Galápagos hotspot. *Geophysical Journal International*, *161*, 763–788. https://doi.org/10.1111/j.1365-246X.2005.02592.x

Sallarès, V., Gailler, A., Gutscher, M.-A., Graindorge, D., Bartolomé, R., Gracia, E., et al. (2011). Seismic evidence for the presence of Jurassic oceanic crust in the central Gulf of Cadiz (SW Iberian margin). *Earth and Planetary Science Letters*, *311*(1), 112–123.

Sallarès, V., Martínez-Loriente, S., Prada, M., Gràcia, E., Ranero, C. R., Gutscher, M. A., et al. (2013). Seismic evidence of exhumed mantle rock basement at the Gorringe Bank and the adjacent Horseshoe and Tagus abyssal plains (SW Iberia). *Earth and Planetary Science Letters*, *365*, 120–131. https://doi.org/10.1016/j.epsl.2013.01.021

Sandwell, D. T., Muller, R. D., Smith, W. H. F., Garcia, E., & Francis, R. (2014). New global marine gravity model from CryoSat-2 and Jason-1 reveals buried tectonic structure. *Science*, *346*(6205), 65–67. https://doi.org/10.1126/science.1258213

Sawyer, D. S., Whitmarsh, R. B., & Klaus, A. (1994). Shipboard Scientific Party. In Proceeding of Ocean Drill. Program, Initial Rep (Vol. 149, pp. 719).

Schettino, A., & Turco, E. (2011). Tectonic history of the western Tethys since the Late Triassic. *Bulletin*, *123*(1–2), 89–105. https://doi.org/10.1130/b30064.1

Sibuet, J.-C., Srivastava, S. P., & Spakman, W. (2004). Pyrenean orogeny and plate kinematics. *Journal of Geophysical Research: Solid Earth*, *109*(B8). https://doi.org/10.1029/2003jb002514

Srivastava, S., Sibuet, J.-C., Cande, S., Roest, W., & Reid, I. D. (2000). Magnetic evidence for slow seafloor spreading during the formation of the Newfoundland and Iberian margins. *Earth and Planetary Science Letters*, *182*(1), 61–76. https://doi.org/10.1016/s0012-821x(00)00231-4

Sutra, E., & Manatschal, G. (2012). How does the continental crust thin in a hyperextended rifted margin? Insights from the Iberia margin. *Geology*, *40*, 139T–142T. https://doi.org/10.1130/G32786.1

Tarantola, A. (1987). Inversion of travel times and seismic waveforms. *Seismic Tomography*, 135–157. https://doi.org/10.1007/978-94-009-3899-1_6

Tucholke, B. E., & Ludwig, W. J. (1982). Structure and origin of the J-Anomaly ridge, Western North-Atlantic Ocean. *Journal of Geophysical Research*, *87*(NB11), 9389–9407. https://doi.org/10.1029/jb087ib11p09389

Tucholke, B. E., Sawyer, D. S., & Sibuet, J.-C. (2007). Breakup of the Newfoundland–Iberia rift. *Geological Society, London, Special Publications*, *282*(1), 9–46. https://doi.org/10.1144/sp282.2

Tucholke, B. E., & Vogt, P. R. (1979). Site 384: The Cretaceous/Tertiary boundary, Aptian reefs, and the J-Anomaly Ridge. *Initial Reports of the Deep Sea Drilling Project*, *43*, 107–165.

Van Avendonk, H. J., Holbrook, W. S., Nunes, G. T., Shillington, D. J., Tucholke, B. E., Louden, K. E., et al. (2006). Seismic velocity structure of the rifted margin of the eastern Grand Banks of Newfoundland, Canada. *Journal of Geophysical Research*, *111*, B11404. https://doi.org/10.1029/2005jb004156

Verhoef, J. H., Collette, B. J., Dañobeitia, J. J., Roeser, H. A., & Roest, W. R. (1991). Magnetic anomalies off West-Africa (20°–38°N). *Marine Geophysical Researches*, *13*, 81–103.

Wessel, P., & Smith, W. (1995). New version of the generic mapping tool released. *EOS, Transactions, AGU*, *76*(33), 329–329. https://doi.org/10.1029/95eo00198

Whitmarsh, R. B., Beslier, M. O., & Wallace, P. J. (1998). Leg 173. In Proceeding of ODP, Init. Rep (Vol. 173, p. 493).

Whitmarsh, R. B., Manatschal, G., & Minshull, T. A. (2001). Evolution of magma-poor continental margins from rifting to seafloor spreading. *Nature*, *413*, 150–154. https://doi.org/10.1038/35093085

Whitmarsh, R. B., White, R. S., Horsefield, S. J., Sibuet, J. C., Recq, M., & Louvel, V. (1996). The ocean-continent boundary off the western continental margin of Iberia: Crustal structure west of Galicia Bank. *Journal of Geophysical Research: Solid Earth*, *101*, 28291–28314, https://doi.org/10.1029/96JB02579

Williams, R. G., & Pollatos, J. (2012). Signal to noise—The key to increased marine seismic bandwidth. *First Break*, *30*(11). https://doi.org/10.3997/1365-2397.30.11.64587

Zelt, C. A., & Forsyth, D. A. (1994). Modeling wide-angle seismic data for crustal structure—Southeastern Grenville Province. *Journal of Geophysical Research: Solid Earth*, *99*(B6), 11687–11704. https://doi.org/10.1029/93jb02764